CHAPTER II

EXPERIMENTAL

As discussed in the literature study in Chapter I, one needs an experimental set-up that will simulate uni-directional heating conditions typical of the industrial process under study. To simulate uni-directional heating in a tube furnace a unique experimental set-up was developed that allows the sample to be transported into and out of the experimental tube furnace heating zone, under a protected atmosphere. This set-up also allows for product gas analyses to be done throughout the experiment. Furthermore the experimental set-up was used to quantify the heat transferred to the sample over the experimental time period.

A standard tube furnace was adapted to connect a sample lifting tube to the bottom lid, attached to the furnace tube. The sample lifting tube contained a pedestal holder that lifted the pedestal into the furnace through a piston action. Radiation shields were positioned inside the top and bottom end of the furnace tube to direct radiation heat to the sample surface, and away from the sample sides. The top lid contained a view port for sample surface temperature measurement. The pedestal contained thermocouples to measure the sample temperature at different positions within the sample. The furnace tube surface, used as radiation heat source to heat the sample surface, was conceptually divided into three heating surfaces. Radiation heat transfer input to the sample surface was increased by increased heat input to the heating surfaces via the furnace heating elements. The furnace temperature control thermocouple was positioned outside the furnace tube, close to the middle of the furnace element heating zone. Increased heat transfer to the sample surface was established by increased furnace control thermocouple set points of 1300°C, 1400°C and 1500°C, respectively. The heating surface temperatures were measured throughout each experiment.

2.1. Experimental Set-up

2.1.1. Furnace

The furnace set-up consisted of an alumina furnace tube, 99.8% purity, 88.9 mm O.D. x 79.4 mm I.D. x 1200 mm, positioned vertically inside a circle of six lanthanum chromite ($LaCrO_3$) heating elements which were placed on a circle radius of 57.5 mm from the furnace tube centre. The top and bottom ends of the alumina tube were sealed gas tight via O-rings contained within each brass lid. The furnace tube was supported via the bottom brass lid, resting on a steel bracket bolted onto the furnace frame. The top lid on the furnace connected to another lid to serve as a reducer and variable seal. Because of thermal expansion of the ceramic furnace tube a variable seal was made between the bolt-on top lid and the rest of the top assembly. The top assembly rested on a bracket bolted onto the tube furnace

frame, as not to rest on the ceramic tube. The position of the top assembly was high enough to accommodate the alumina tube expansion at 1600°C hot zone temperature, but low enough to seal the furnace tube off at room temperature. **Fig. 4** shows to top assembly schematically.

Fig. 4: Top Assembly

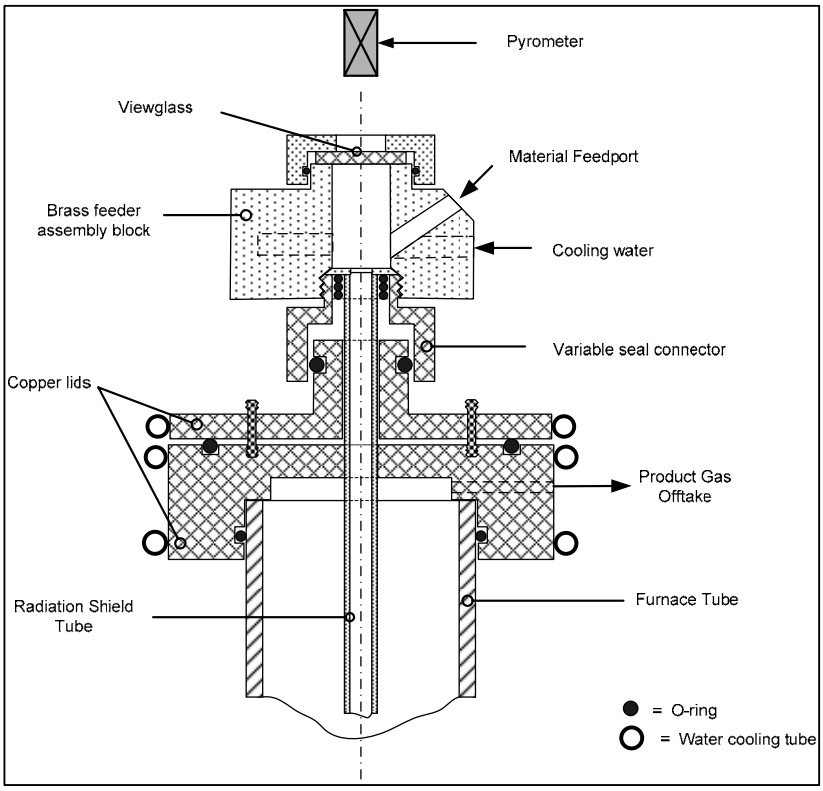

The top radiation shield consisted of a fibreboard disk pasted onto the end of a 20 mm o.d. x 15 mm i.d. mullite tube. The top end of the radiation shield tube was gripped by O-rings contained within the top assembly to keep it in position. The tube also served as the view hole guide. The positioning of the radiation shields relative to the tube furnace refractories is shown in **Fig. 5**. A slide-gate assembly was attached to the bottom lid of the furnace tube, **Fig. 6**. The sample lifting tube in turn was attached onto the bottom end of the slide gate, **Fig. 7**. The sample lifting tube contained a ceramic fibreboard pedestal mounted in an aluminium holder. Four type-K thermocouples were placed within the pedestal on a 5 mm radius, **Fig. 9**. The thermocouple wires, of ~ 0.4 mm diameter housed in twin bore alumina tubes of 2.2 mm o.d., exited the pedestal at the bottom end of the aluminium pedestal holder. The wires were coiled within the free space below the aluminium pedestal holder so that they may uncoil as the pedestal holder is lifted up inside the aluminium tube by Ar gas. The aluminium pedestal holder functioned as a piston inside the aluminium tube by sliding on two o-rings contained in radial grooves at the bottom and top ends of the aluminium pedestal holder. A stopper ring at the top of the aluminium tube stopped the aluminium pedestal holder at the predetermined travel distance. The

sample was lifted into the furnace by letting Ar gas flow into the bottom end of the sample tube, via a control valve set at 50 kPa gauge pressure. When the sample reached the top of the travel position into the furnace, the sample surface level was flush with the bottom radiation shields' top surface. To lower the sample into the sample tube the Ar gas was pumped out of the tube by a vacuum pump.

Fig. 5: Furnace layout

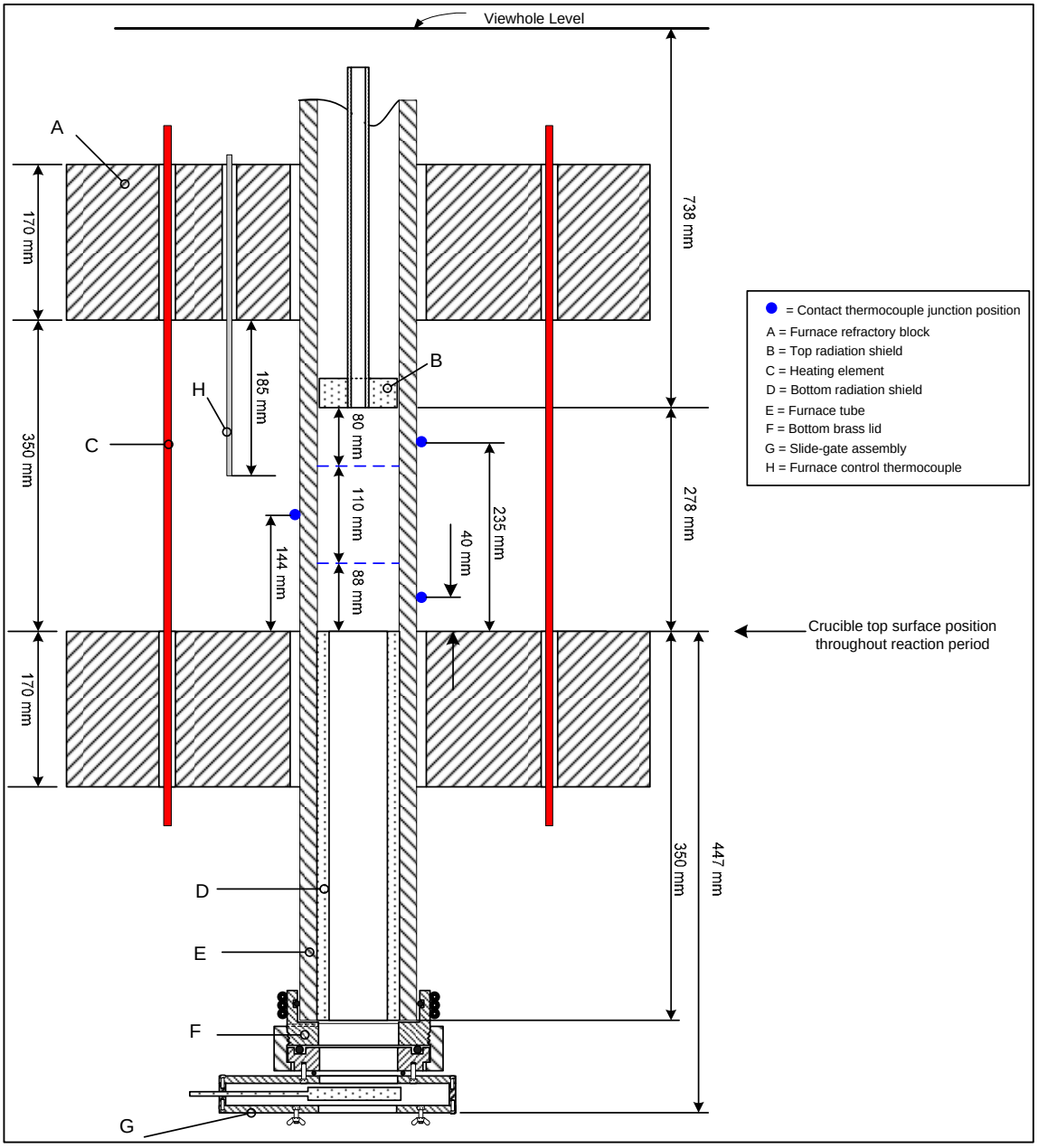

The wires exited the sample tube via a sealed fitting and the thermocouple outputs were logged with a dataTaker DT500 logger at one-second intervals. The sample crucible, shown in **Fig. 8**, was made from ceramic fibreboard and sat on top of the pedestal, with type-K thermocouples entering the sample

through the crucible bottom. The crucible dimensions were 30 mm i.d., 50 mm o.d. and the crucible bottom was either 10 or 24 mm thick. The crucible was filled with material mixture so that the sample surface and the crucible top surface were level. The sample tube contained two fibreboard insulation rings, within its wider top section, to protect the aluminium when the hot sample was lowered into the sample tube. The sample tube assembly could be flushed via an Ar gas inlet and outlet on the sample tube, each line fitted with a ball valve. The furnace was flushed with Ar gas entering through the bottom brass lid, and exiting through the top brass lid. The furnace tube contained a cylindrical fibreboard radiation shield made from individual fibreboard rings cemented onto each other. This radiation shield rested on the bottom brass lid.

Fig. 6: Furnace Tube Bottom Assembly (Bottom lid & slide gate)

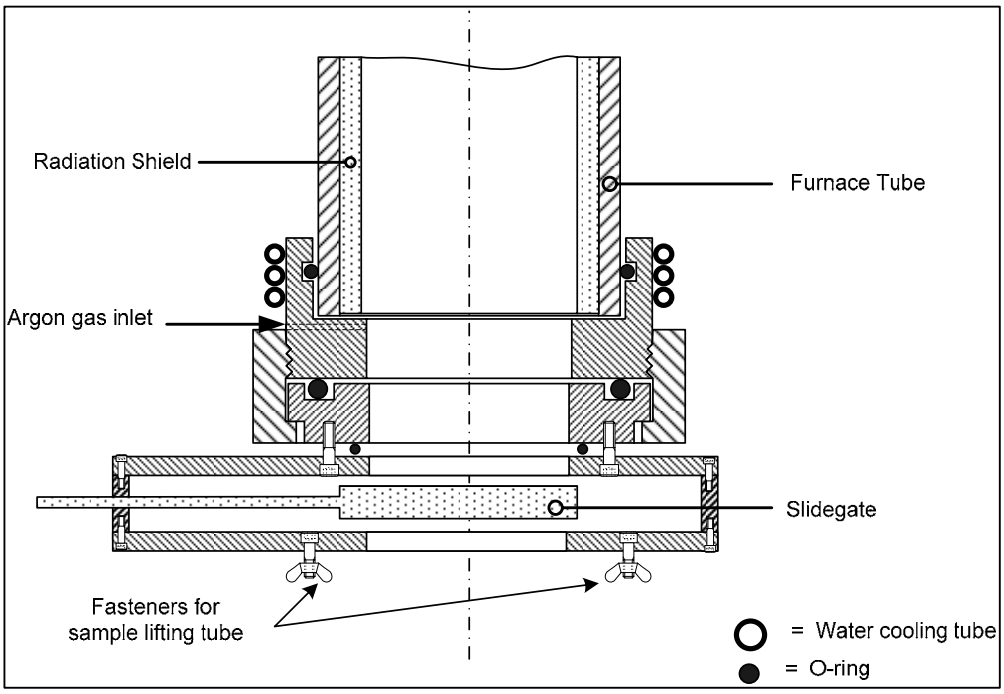

Fig 7: Sample Tube with Pedestal

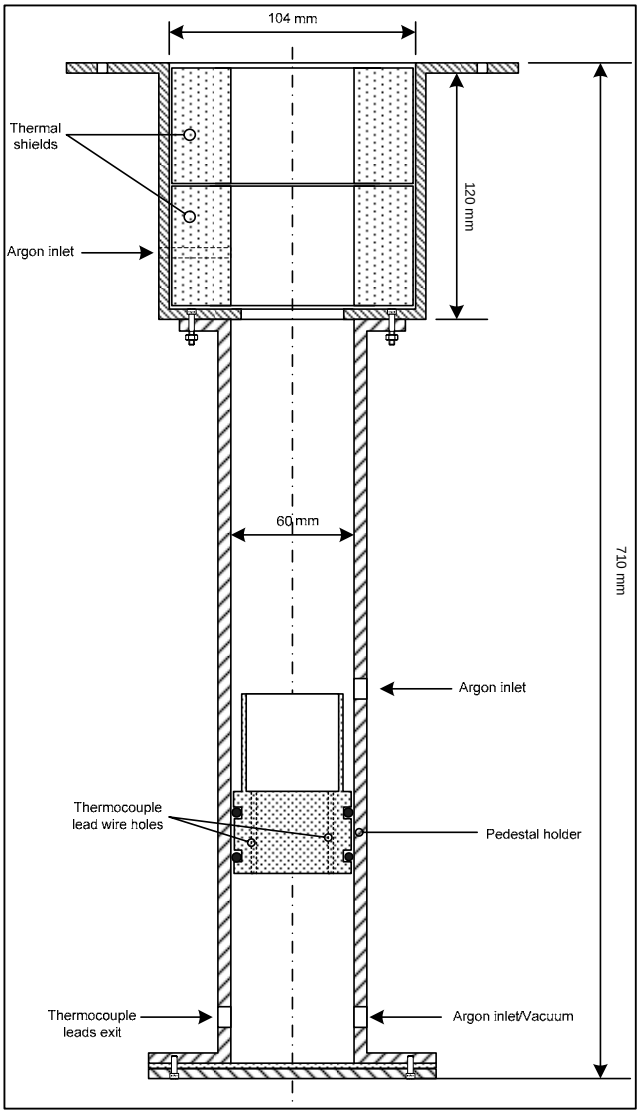

Fig. 8: Crucible

Fig. 9: Pedestal and thermocouples

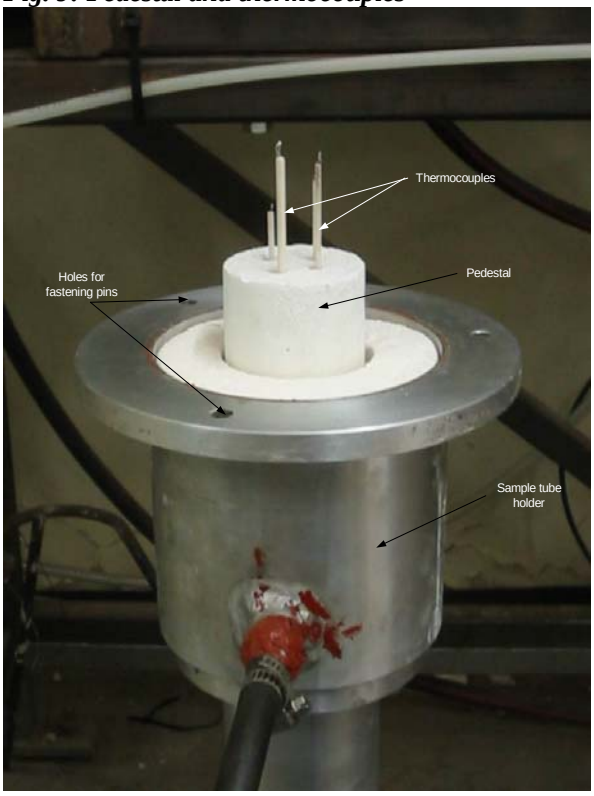

The furnace temperature was controlled by a PID controller/programmer using a type-B thermocouple positioned next to the furnace tube, radially close to the hot zone, and vertically close to the middle of the furnace element heating zone. The hot zone position was measured by placing a hand held type-S thermocouple at various depths into the furnace tube. The thermocouple was kept at one position for two minutes, and then moved to the next position. The measurements are shown **Fig. 10**, with the certified standard deviation range for the thermocouple wire. The 0 cm reference point was the top surface of the top assembly when the view glass holder was removed.

Fig. 10: Hot zone measurements

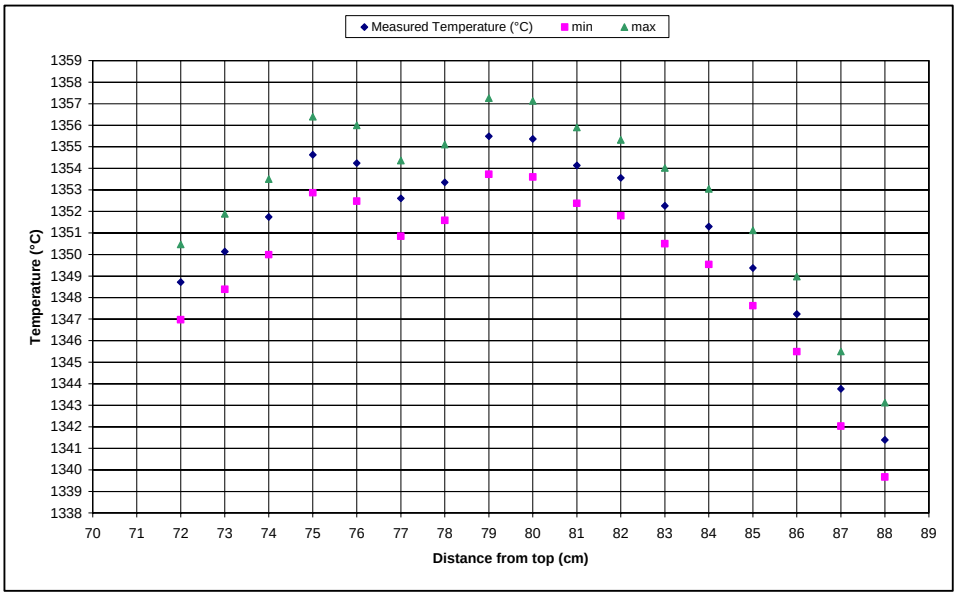

Initial efforts to use a 87 mm heating zone around the hot zone centre, at 784 mm from 0 reference level, was not successful as the bottom radiation shield could not shield the sample sides sufficiently from radiation heat from the furnace tube. This was because the total heating length of the furnace is 350 mm in length, see **Fig. 5**. Thus, the heating zone was enlarged to include the section of furnace tube extending from the bottom of the hot zone to the top of the external furnace refractory. This second heating zone was conceptionally divided into two sections. The heating zone thus consists of three sections, the furnace tube length of 80 mm around the furnace hot zone, and the second and third sections of 110 mm and 88 mm length, respectively, extending below the first heating zone. The heating surface temperatures of each of the three heating sections were measured throughout each experiment by type-S contact thermocouples placed on the furnace tube exterior surface, as shown in **Fig. 5**. Uni-directional heat transfer along the vertical axis of the crucible and contents was confirmed by viewing polished sections of reacted samples under reflected light, which showed that no reaction fronts existed across the horisontal axis of the crucible contents.

2.1.2. Gas Lines

The supply lines to the furnace and the gas off-take lines from the furnace to the quadropole mass spectrometer (Gaslab) are shown diagrammatically in **Fig. 11**. Argon gas of 99.999% purity was used as carrier gas. The Ar gas was cleaned by passing through anhydrous $CaSO_4$ to remove water ("Drierite"), and through an "Oxyzorb" cartridge to remove oxygen. The carrier gas was passed through the experimental set-up at ~1500 Ncm^3/min. The Ar flow rate was measured before each experiment sequence using a bubble meter, and the flow was controlled by a Rotameter fed from the Ar bottle via a pressure regulator.

The product gas was passed through a Balston filter (050-11 DX) to remove small solid particles from the gas. The gas flowed past a draw off point for the mass spectrometer (Gaslab), and then through a bubbler to the vent. The gas system was also used to calibrate the mass spectrometer for Ar, CO_2, CO, CH_4 and H_2 by connecting the particular calibration gas supply to the one-way inlet valve connection shown in **Fig. 11**. The calibration gases used were 100%CO, 5%CH_4-Ar, 5%H_2-Ar, 100%Ar and 10%CO_2-Ar, respectively. Calibration for Ar and CO_2 was done by using the furnace gas supply lines up to the one way inlet valve connection, **Fig. 11.**

The product gas water content was measured by a Dewmet cooled mirror dewpoint meter. The product gas off-take lines, 6 mm o.d. copper tubing, were heated by trace heating to prevent condensation of water from the product gas. A type-K thermocouple was placed in the heated line to monitor the gas temperature. These temperature values were typically between 120-135°C. This K-type thermocouple measurement was pre-calibrated to the gas temperature measured with a thermometer at the dewpointmeter chamber gas inlet. At 1300°C furnace temperature the gas temperature measured at the dewpoint chamber inlet was 76°C for type-K thermocouple measurement of 133°C. The type-K thermocouple was used as an indicator temperature to prevent overheating the Dewmet sensor.

The Ar gas used for initial flushing of the sample holder, to displace the bulk of air in the sample holder and furnace tube, was also 99.999% pure Ar taken from a separate cylinder, and passed through "Drierite". The gas sampling response time could best be determined from devolatilisation experiments. This is because devolatilisation starts at a few hundred degrees so that sample gas evolution is immediate when the sample is lifted into the furnace tube, and so provided a definitive start time for gas evolution against which the response time to the first analyses of the devolatilisation product gas could be measured. The sampling delay time at ~1500 Ncm^3/min was found to be 11-12 seconds from zero time. Zero time is the time at which the sample has reached the top of the travel position into the furnace tube. The 11-12 seconds is the fastest analysis interval time achieved by the mass spectrometer for the analyses set-up selected on the mass spectrometer. For the Dewmet the sampling response time was 22-24 seconds. The time to lift the sample up into the furnace, or lower the sample into the sample holder, was approximately 5 seconds. The flow rate of product gas components was calculated by scaling relative to the input Ar flow rate, as shown in **Appendix I**.

The maximum gas retention time in the furnace tube open volume was calculated to be 159 seconds for a volume of 3892 cm^3 and Ar gas flow rate of 1500 Ncm^3/min. The minimum gas retention time in the furnace tube was calculated as ~ 30 seconds, assuming the gas was heated to the sample surface temperature. The time period required for the product gas analysis to return to that before the sample was lifted into the furnace tube, was noted from the product gas analyses. This data is expressed, for each product gas component, as a multiple of the gas retention time in the furnace tube open volume.

$$t_m = \frac{(t_s - t_l)}{t_r} \quad (7)$$

t_m = Time multiple for product gas to return to product gas composition at start of experiment [seconds]
t_s = Time when product gas analysis return to product gas composition at start of experiment [seconds]
t_l = Time when sample was lowered from furnace tube [seconds]
t_r = Maximum gas retention time in the furnace tube open volume [seconds]

For the samples of graphite and pre-reduced Sishen iron ore the time multiples varied from -8 to +5. The negative values are possible when the component in the product gas return to the initial levels before the sample is lowered from the furnace tube. For the ore-coal samples the time multiples varied from -1 to 8, and in two experiments the CO analyses did not return to the initial level. The data for calculation of the time multiple is summarized in **Appendix I**.

The furnace assembly was checked for gas leaks by drawing vacuum of 80 kPa on the assembly, if this vacuum was maintained, the assembly was considered gas tight. The sample holder was checked for gas leaks by passing gas through the assembly, and using soap water to identify leaks.

Fig. 11: Gas supply and off-take lines to/from furnace

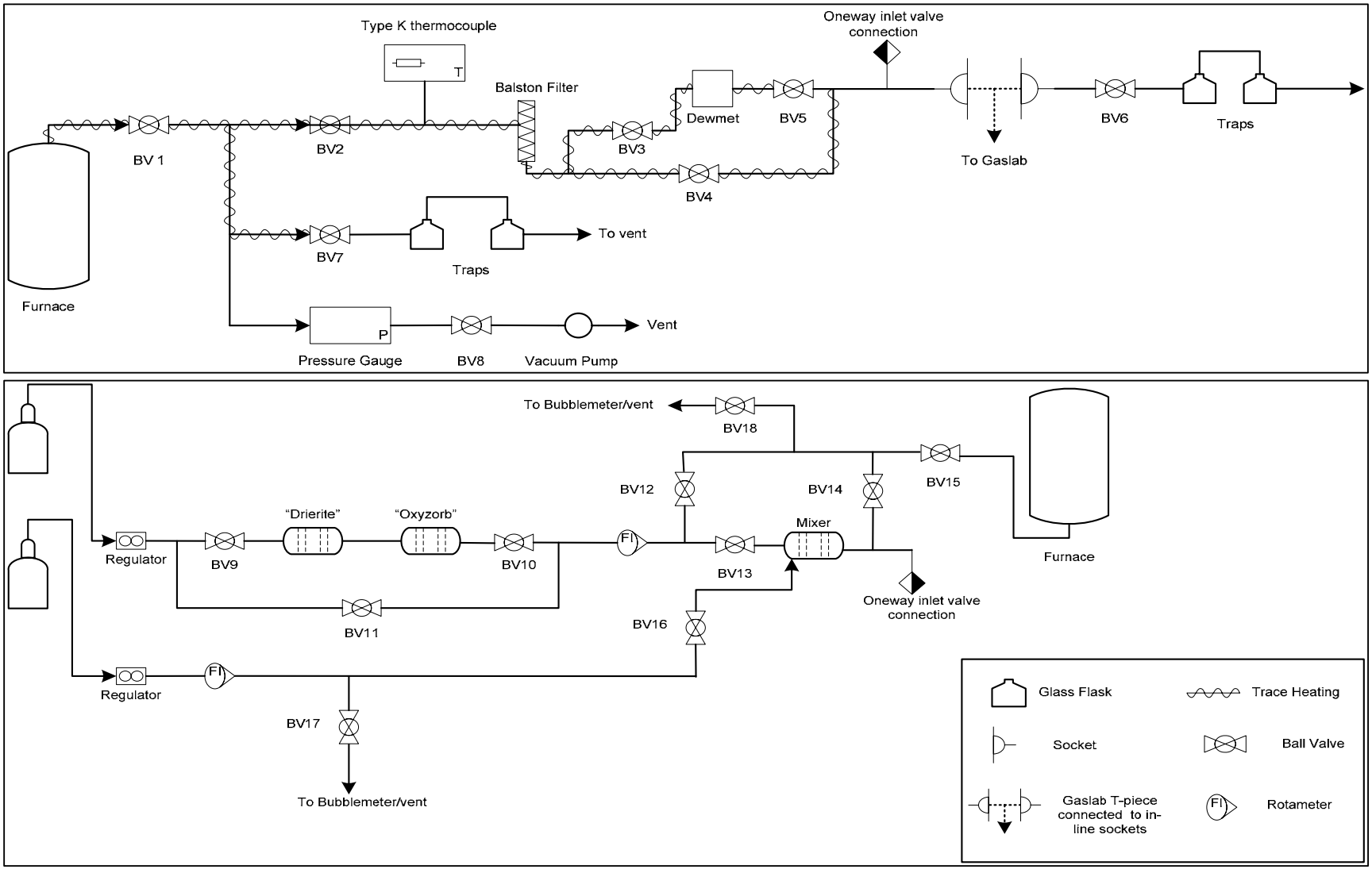

2.2. Calibration

2.2.1. Radiation Network

The radiation heat transfer set-up in the tube furnace is shown in **Fig. 12**. The heat transferred to the sample surface can be calculated from a radiation network representing the heat flows in the experimental set-up. The network is shown in **Fig. 13** and was developed according to the formalism set out in Holman (1992), p. 410-413. Calculation of the view factors is summarised in **Appendix II**. The calculations are outlined below. In **Fig. 12** two imaginary surfaces 8 and 7 are used to calculate the shape factors for use in the radiation network calculations. The symbols shown in **Fig. 13** are defined as follows: J_i = radiosity of surface i = total radiation that leaves surface i per unit time per unit area [kW/m^2]; R_i = Resistance i in radiation network [m^{-2}]; $E_{bi} = \sigma T^4$ = blackbody emissive power of surface i [kW/m^2]; σ = Stefan-Boltzmann constant = 5.669 x 10^{-8} W/m^{2}K^4.

Fig. 12: Radiation Configuration

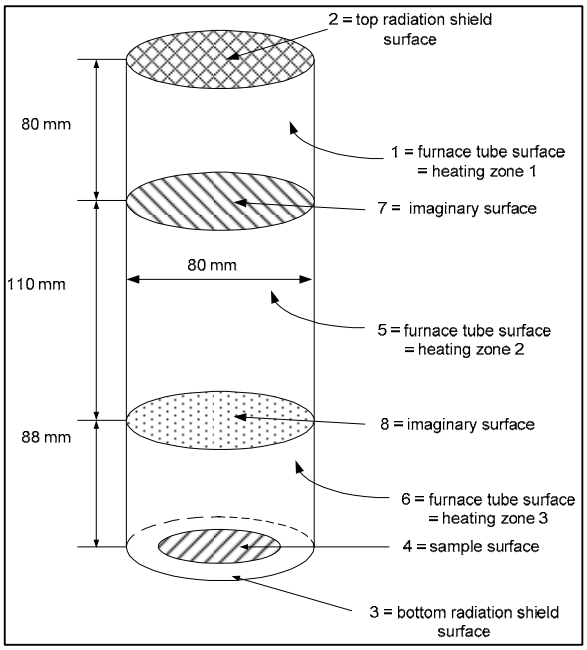

Fig. 13: Radiation Network

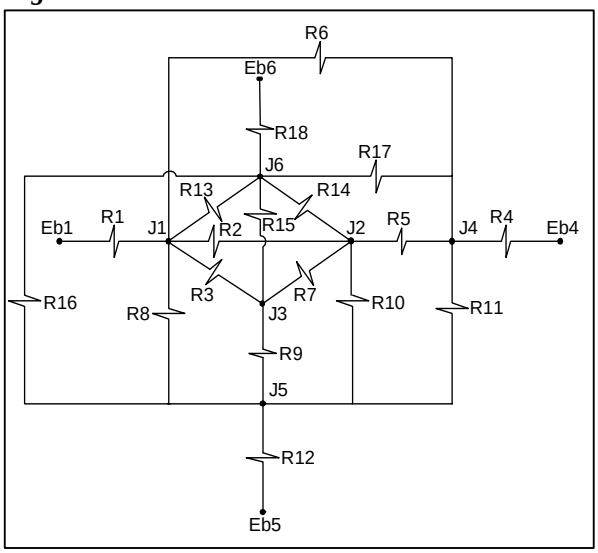

2.2.1.1. Resistances

The radiation network resistances in **Fig. 13** were calculated as follows:

For the surface resistances of surfaces 1, 4, 5 and 6:

$$R_1, R_4, R_{12}, R_{18}: \; R_i = \frac{1-\varepsilon_j}{\varepsilon_j A_j} \tag{8}$$

R_i = Resistance *i* in radiation network
ε_j = Emissivity of surface *j* in radiation network
A_j = Area of surface *j*

For the space resistances:

$$R_2, R_3, R_5, R_6, R_7, R_8, R_9, R_{10}, R_{11}, R_{13}, R_{14}, R_{15}, R_{16}, R_{17}: \; R_n = \frac{1}{A_i F_{ij}} \tag{9}$$

F_{ij} = View factor for radiation from surface *i* to surface *j*
A_i = Area of surface *i*

2.2.1.2. Node Equations

The temperatures for surfaces 1, 4, 5 and 6 are known and the radiosity of the six nodes must be calculated from the node equations. The following node equations were generated according Kirchhoff's rule. The equations are solved numerically for the radiosities (J_i).

Node 1:

$$\frac{E_{b1}-J_1}{R_1}+\frac{J_2-J_1}{R_2}+\frac{J_3-J_1}{R_3}+\frac{J_4-J_1}{R_6}+\frac{J_5-J_1}{R_8}+\frac{J_6-J_1}{R_{13}}=0 \tag{10}$$

Node 2:

$$\frac{J_1-J_2}{R_2}+\frac{J_3-J_2}{R_7}+\frac{J_4-J_2}{R_5}+\frac{J_5-J_2}{R_{10}}+\frac{J_6-J_2}{R_{14}}=0 \tag{11}$$

Node 3:

$$\frac{J_1-J_3}{R_3}+\frac{J_2-J_3}{R_7}+\frac{J_5-J_3}{R_9}+\frac{J_6-J_3}{R_{15}}=0 \tag{12}$$

Node 4:

$$\frac{E_{b4}-J_4}{R_4}+\frac{J_1-J_4}{R_6}+\frac{J_2-J_4}{R_5}+\frac{J_5-J_4}{R_{11}}+\frac{J_6-J_4}{R_{17}}=0 \tag{13}$$

Node 5:

$$\frac{E_{b5}-J_5}{R_{12}}+\frac{J_1-J_5}{R_8}+\frac{J_2-J_5}{R_{10}}+\frac{J_3-J_5}{R_9}+\frac{J_4-J_5}{R_{11}}+\frac{J_6-J_5}{R_{16}}=0 \quad (14)$$

Node 6:

$$\frac{E_{b6}-J_6}{R_{18}}+\frac{J_1-J_6}{R_{13}}+\frac{J_2-J_6}{R_{14}}+\frac{J_3-J_6}{R_{15}}+\frac{J_4-J_6}{R_{17}}+\frac{J_5-J_6}{R_{16}}=0 \quad (15)$$

The heat transferred to the sample surface is then calculated:

$$q_4=\frac{E_{b4}-J_4}{R_4A_4}\ [\mathrm{kW/m^2}] \quad (16)$$

2.2.2. Emissivity Measurements

The emissivities of alumina powder, alumina furnace tube material, fibre board and fibre board coated with alumina paste were measured by placing the materials in a muffle furnace to heat up with the furnace to 999, 1104, 1208 and 1306°C, respectively. A hand held type-S thermocouple was used to check that the furnace temperature is at the furnace temperature set on the furnace PID controller. The different material temperatures were measured by opening up the muffle furnace door and measuring the sample temperature with an optical pyrometer, Minolta/Land Cyclops 152A infrared thermometer, with the emissivity on the pyrometer set at 1.00. The measurements were logged with a dataTaker DT500 logger at one-second intervals. After a measurement was made on one of the four materials, the muffle furnace was closed to allow it to attain the set temperature again, before the next material sample temperature was measured. The main assumption is that the material samples in the muffle furnace are at the furnace temperature when the pyrometer temperature measurement is made. Equation 17, the Planck blackbody radiation law, was used to back calculate the sample material emissivity required to set the material sample surface temperature equal to the furnace temperature (T_r). The other variable in the calculation is the spectral response of the Minolta/Land Cyclops 152A infrared thermometer at 0.8-1.1µm. Calculations were done for both the upper and lower limit wavelength of the pyrometer spectral response, but the emissivity values calculated for 0.95µm at 1306°C furnace temperature were used in further calculations. The temperature measurements are summarised in **Table 4**. The emissivities calculated at different wave lengths are summarised in **Table 5**.

Table 4: Temperature measurements with pyrometer emissivity set to 1.00

Furnace Temperature (°C)	Alumina powder	Alumina furnace tube	Fibre board	Fibre board coated with alumina paste
999	946.3	946.0	960.3	942.1
1104	1032.1	1047.0	1036.6	1032.1
1208	1126.8	1146.0	1131.3	1121.1
1306	1204.8	1244.8	1208.2	1210.8

Table 5: Emissivities calculated at different wavelengths

Furnace Temperature (°C)	Alumina powder			Alumina furnace tube			Fibre board			Fibre board coated with alumina paste		
Wavelength (μm) →	**0.80**	**0.95**	**1.10**	**0.80**	**0.95**	**1.10**	**0.80**	**0.95**	**1.10**	**0.80**	**0.95**	**1.10**
999°C	0.54	0.60	0.64	0.54	0.59	0.64	0.64	0.69	0.72	0.51	0.57	0.61
1104°C	0.49	0.55	0.59	0.57	0.62	0.66	0.51	0.57	0.61	0.51	0.55	0.59
1208°C	0.49	0.55	0.60	0.59	0.64	0.68	0.52	0.57	0.62	0.47	0.53	0.58
1306°C	0.46	0.52	0.57	0.63	0.68	0.72	0.48	0.53	0.59	0.48	0.54	0.59

2.2.3. Sample Surface Temperature Measurement

One of the main input parameters into the radiation network calculation is the sample surface temperature. In the experiments the sample surface temperature was measured with a Minolta/Land Cyclops 152A infrared thermometer with spectral response of 0.8-1.1μm. The measurement was made through a view glass, along a 15 mm i.d. tube, 738 mm in length. The view glass consisted of 4mm thick Robax® glass with transmissivity of 0.88 at 1.1μm and 0.91 at 0.8μm. To check the accuracy of the sample surface temperature measurement made with the pyrometer, the actual surface temperature of an inert alumina powder sample was measured with a type-S thermocouple positioned 5 mm from the sample surface. The sample was introduced into the furnace, and once the sample temperature stabilised, sample surface temperature measurements were made simultaneously using the type-S thermocouple and the pyrometer.

The pyrometer emissivity was set at 1.00 for the pyrometer sample surface temperature measurement. This measured temperature value (T_m) was then corrected for the actual alumina powder emissivity of 0.52 reported in **Table 5**, and glass transmissivity if applicable, using equation 17. Initial measurements were made with and without the view glass, and with and without Ar purging gas, at 1300, 1400 and 1500°C furnace hot zone temperatures, respectively. Measurement with Ar purging gas flow through the furnace tube resulted in a maximum decrease of 5°C in sample surface temperature, at 1500°C furnace hot zone temperature. Comparisons were made for measurements through the view glass with Ar gas flow through the furnace. The same alumina sample mass was used in each experiment. The measurement for 1300°C furnace temperature was repeated. The change in

sample and surface temperatures for the two tests at 1300°C furnace temperature, as well as for 1400°C and 1500°C furnace temperatures are shown in the graphs in **Appendix III**. It is seen that the sample was positioned in the furnace for 50 minutes, or more, to stabilise the sample temperatures. For measurements made at 1500°C furnace temperatures some interference with the thermocouple measurements was experienced. The filtered values are shown in the first graph, for measurements at 1500°C, in **Appendix III** and both the filtered and original data are shown in the following graph. It was determined that the interference occurred with the heating cycles of the furnace elements, therefore only the values at the end-point were checked by switching the furnace off. The end-point temperatures measured by the type-S thermocouple and the pyrometer, respectively, are shown in **Table 6**. The sample surface temperatures as adjusted for the emissivity setting on the pyrometer and the view glass transmissivity are also shown in **Table 6**. The pyrometer sample surface temperature measurement over reads the sample surface temperature by 6°C at 1300°C furnace temperature, and under reads 14°C at 1500°C furnace temperature. The effect of the pyrometer over and under reading of the alumina sample surface temperature on heat transferred to the sample surface is shown by comparison of the kW/m^2 transferred to the alumina sample surface, calculated using the radiation network set out in 2.2.1., using as input the sample surface temperature measured with the type-S thermocouple vs. the sample surface temperature measured with the pyrometer. In the radiation network calculation the sample surface temperatures shown in **Table 6** were used with the associated heating zone temperature values at the end of the heating period. The resultant differences in radiation heat transfer calculation values are summarised in **Table 6**. Heat transfer calculation values vary from under calculation of 4kW/m^2 at 1300°C furnace temperature to over calculation of 13kW/m^2 at 1500°C furnace temperature.

Table 6: Sample surface measurements

Furnace Hot Zone Temperature (°C)	Pyrometer measurement (°C); ε = 1.00	S-type thermocouple measurement (°C)	Adjusted Pyrometer measurement (°C) @ 0.95 µm	ΔT[a]	*kW/m^2 into alumina sample	ΔkW/m^2 for alumina sample[b]
1300a	1076	1172	1177	-6	-61	-3
1300b	1082	1178	1184	-6	-59	-4
1400	1172	1290	1288	2	-73	2
1500	1250	1394	1380	14	-93	13

[a] (S-type thermocouple measurement) – (Adjusted Pyrometer measurement)
* kW/m^2 calculated from S-type thermocouple surface temperature measurement
[b] (kW/m^2 calculated using the S-type thermocouple measurement as sample surface temperature) – (kW/m^2 calculated using the adjusted Pyrometer measurement used as sample surface temperature).

$$T_r = \frac{C_2}{\lambda} \cdot \frac{1}{ln(\frac{C_1}{\lambda^5 E_b} + 1)} - 273 \quad (°C) \tag{17}$$

$$E_b = \frac{E_{app}}{\varepsilon \tau} \tag{18}$$

$$E_{app} = \frac{C_1}{\lambda^5} \cdot \frac{1}{e^{\frac{C2}{\lambda T_m}} - 1} \qquad (19)$$

$C_1 = 3.743 \text{ x } 10^5 \text{ kW } \mu m^4/m^2$
$C_2 = 1.4387 \text{ x } 10^4 \ \mu m \text{ K}$
$\lambda =$ wavelength (μm)
$\varepsilon =$ emissivity
$\tau =$ transmissivity
$T_m =$ Temperature measured by pyrometer (K)
$T_r =$ Real Temperature (°C)
$E_b =$ Black body emissive power per unit wavelength [kW/μm m^2]
$E_{app} =$ Apparent body emissive power per unit wavelength [kW/μm m^2]

2.2.4. Calibration of Radiation Network Calculation

To calculate the heat transferred to the sample one must know the relevant surface temperatures, that is the average furnace tube temperature for each heating zone and the sample surface temperature. As shown in the furnace layout diagram in **Fig. 5**, the section of the furnace tube used as heating surface is 278 mm in length, compared with the typical tube furnace hot zone length of ~ 80 mm. Therefore, the heating surface is not at one temperature and the variation in temperature over the total 278 mm length of heating surface is required as input to the radiation calculation. Consequently the heating surface was divided conceptionally into three heating zone sections to add resolution to the radiation network calculation. The temperature at the vertical centre of each heating zone was measured by placing a contact thermocouple at the outside surface of the furnace tube at a position 5 mm below the heating zone centre. The 5 mm allowance was made to account for the furnace tube expansion.

In addition to the three heating zone surface temperatures, the sample surface temperature was measured by pyrometer, through the view glass at the top of the experimental assembly. These temperatures were used as inputs to the radiation network calculation. The sample surface temperature was measured with the pyrometer emissivity setting at 1.00, and the measurements were then corrected for view glass transmissivity of 0.88 and sample material emissivity of 0.90 at 0.95μm wavelength, using equation 17.

To calibrate the radiation network samples of pre-reduced Sishen ore and graphite were reacted at 1300, 1400 and 1500°C, respectively. This selection of materials was made to simplify the possible reactions, as compared to coal and unreduced Sishen fines. The graphite and pre-reduced Sishen ore were of -850 +425μm size fraction. Chemical analyses for these materials and XRD (X-ray diffraction) analysis for the pre-reduced ore are shown in **Appendix IV**. After the runs the reacted samples were sectioned horizontally into three portions, and analysed for forms of Fe, %C by Leco

method, and main components by ICP (Inductively coupled plasma) method. As a check on the chemical analyses control samples were prepared from pre-reduced ore and graphite at different carbon contents. Theses samples were submitted for analyses, and the resultant analyses compared with the calculated %C and forms of Fe from the input material analyses. Control samples were also prepared from coal and pre-reduced ore. The comparison for %C in the sample mixtures is shown in **Fig. 14 (a)** for graphite and **Fig. 14 (b)** for coal. It is seen that the %C analysed for the mixtures containing graphite corresponds well. For the coal containing samples it is seen that the total carbon content is analysed, that is fixed carbon and carbon in the volatiles. The analyses and calculated total carbon values differ by a maximum of 1.5%. The forms of Fe analyses are summarised in **Table 7**.

Fig. 14: Comparison of %C in control sample and %C analyses

(a) Graphite

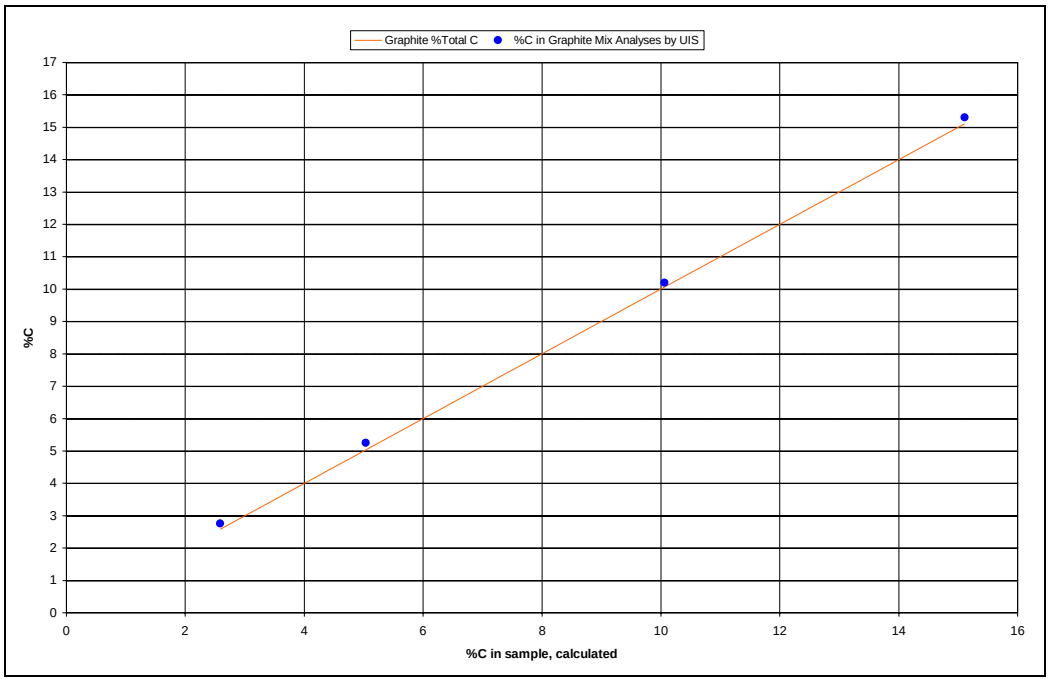

(b) Coal

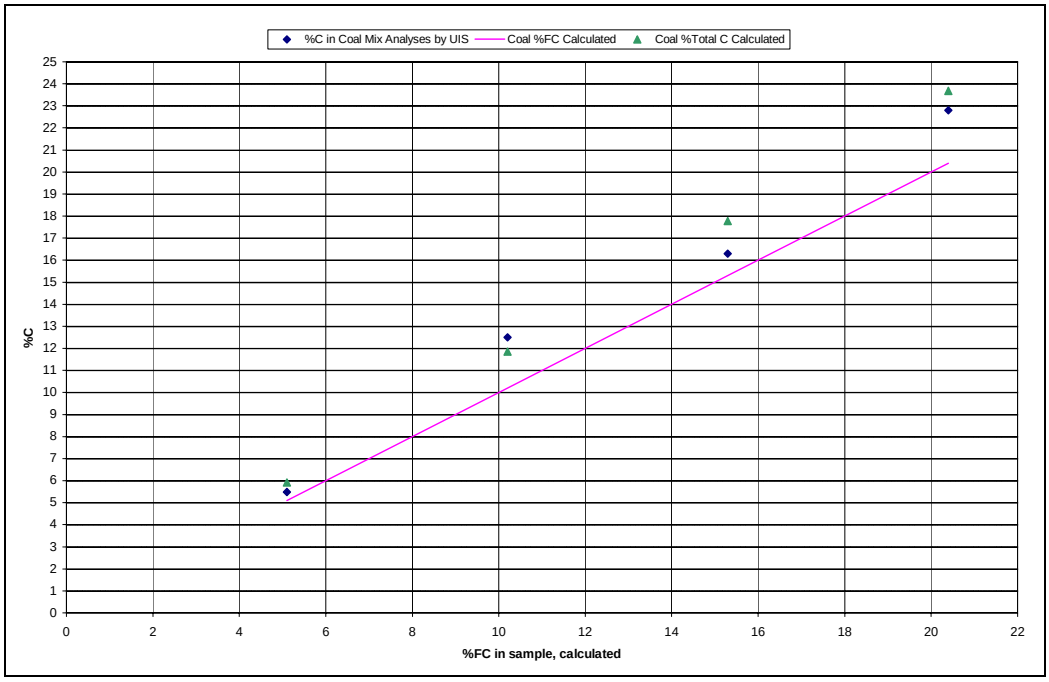

Table 7: Comparison of Forms of Fe from analyses of control samples and input materials.

%C in Graphite-Pre-reduced ore mixture	Fe(total)	Fe^0	FeO	Fe_2O_3
2.5	70.3 / 70.4*	0.24 / 0.18	73.6 / 74.0	19.0 / 18.0
5.0	68.5 / 68.7	0.24 / 0.23	71.7 / 71.9	18.5 / 18.0
10.0	64.8 / 64.9	0.23 / 0.24	67.8 / 68.0	17.5 / 16.8
15.0	61.2 / 60.9	0.21 / 0.28	64.0 / 63.6	16.5 / 15.9
%Fixed Carbon in Coal-Pre-reduced ore mixture	Fe(total)	Fe^0	FeO	Fe_2O_3
5.0	66.5 / 67.7	0.23 / 0.25	69.6 / 71.6	18.0 / 16.8
10.0	60.9 / 62.4	0.21 / 0.29	63.6 / 62.4	16.5 / 19.4
15.0	55.2 / 55.3	0.19 / 0.42	57.6 / 57.8	15.1 / 14.2
20.0	49.6 / 49.6	0.17 / 0.45	51.7 / 52.9	13.6 / 11.4

* Input value/Analysed value

In the reacted sample each of the three horizontal portions can be associated with temperature data measured throughout the experiment by the type-K thermocouples embedded within the sample, at different heights. From the end-point analyses and temperatures a mass balance calculation is made for each horizontal section of the sample (node). Summation of the heat transferred into the sample, as calculated from the heat-mass balance, must correspond to the radiation network calculation that uses only the sample surface temperature, and furnace tube heating zone temperatures as inputs. A schematic representation of the sample nodes and thermocouple positions is shown in **Fig. 15**.

Fig. 15: Crucible, thermocouple positions and node divisions

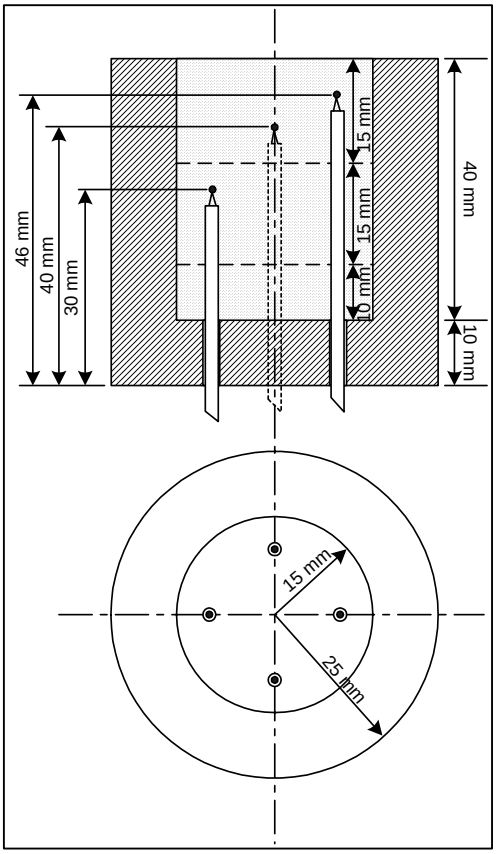

To ensure that all the samples were consistently separated into the three horizontal portions, a sample cutter-splitter was developed as shown in **Fig. 16**. This equipment enables the sample to be separated into the required three portions even if the thermocouples are sintered into the sample, thus cutting through the thermocouple sheath. To test repeatability of the sample cutting method, ten samples of sand were divided into three nodes each and the resultant portions of silica sand nodes and fibre board crucible were then weighed. The detailed mass measurements are summarised in **Appendix V**. The crucible was vertically positioned in the sample cutter to attain the sample divisions so that the top two nodes would respectively take up more of the total sample mass than the bottom node, as the bottom node will be least reacted, and thus of less importance in chemical analyses. Also, the sample material contracts as the sample reacts so that the sample division results in the top node material mass being proportionately less of the total sample mass with increased sample reaction extent. The maximum sample bed height contraction observed visually was 2 mm for coal-ore, coal-char and graphite-ore samples, and maximum 5 mm contraction for coal-alumina samples. The average mass% distribution for the top, middle and bottom nodes is 46, 33 and 21% with 95% confidence limits of 1.0, 0.3 and 0.9%.

Fig. 16: Sample Cutter-Splitter

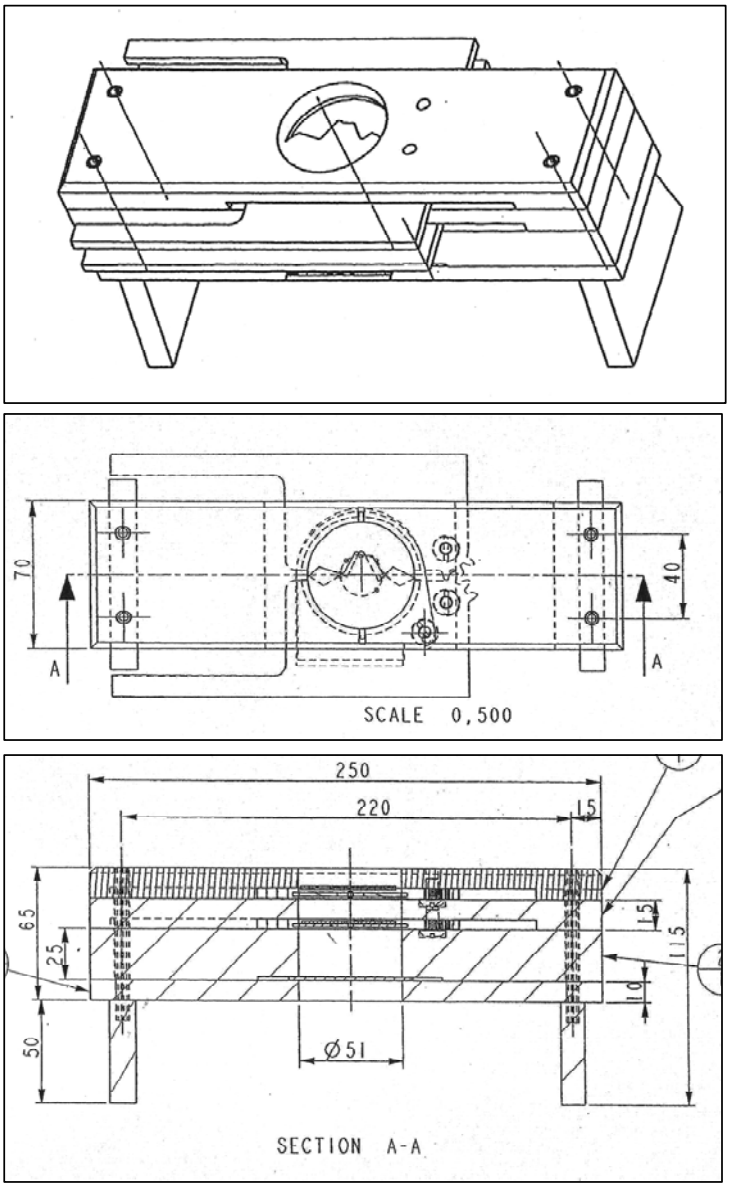

Fig. 17, 18 and 19 a-c shows the heating zone temperatures, sample surface temperatures and internal sample temperatures, as well as the product gas analyses for calibration experiments at furnace hot zone setpoint temperatures of 1300°C, 1400°C and 1500°C. It is seen that the temperatures of the hot zone, heating zone 1, and the heating zone 2 temperatures are within 20°C of each other. The hot zone temperatures and heating zone 3 temperatures differ by as much as 82°C for 1305°C hot zone temperatures, and the biggest difference is at the beginning of the experiment when heating zone 3 temperatures are lower. For each of the 1 second intervals at which temperatures were logged, the radiation heat transferred to the sample was calculated with the hot zone (heating zone 1), second and third heating zone temperatures, and the sample surface temperature measured by infrared pyrometer

as inputs to the radiation network. The weighted average radiation heat transfer value over the experimental period was then used for comparison with the weighted average energy input to the sample as calculated from the incremental heat-mass balance. Because of the one second interval logging of temperature values, the weighted average radiation heat transfer value and the average radiation heat transfer value is the same.

For samples 1300A and 1300B the heating zone 1 temperature values were scattered due to a loose connection to the logger. This temperature corresponds to the hot zone temperature of the furnace, and is therefore close to the controller set point, as is seen for the 1400C, 1400D, 1500E and 1500F samples in **Fig. 18 (a) and 19 (a).** The scatter values below 1300°C were filtered out, and the removed scatter values were then replaced with the average of the values that remained after the filtering step. These values are shown in **Fig. 17 (a).**

Fig. 17: Calibration Measurements at 1300°C Hot Zone Temperature

(a) Heating Zone Temperatures (1300A)

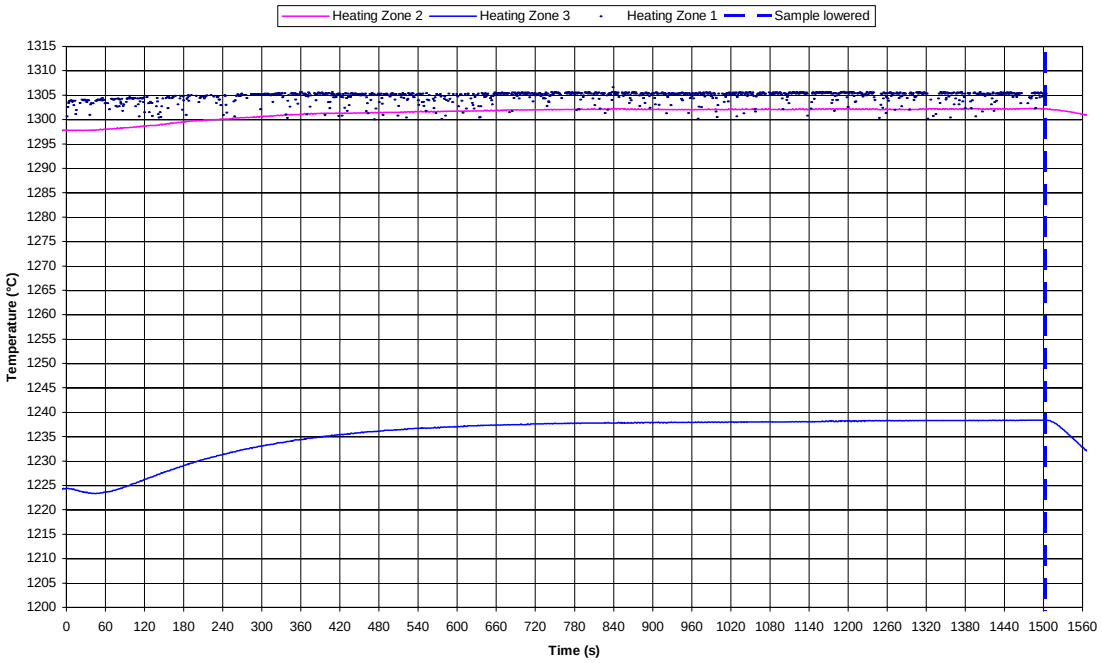

(a) Heating Zone Temperatures (1300B)

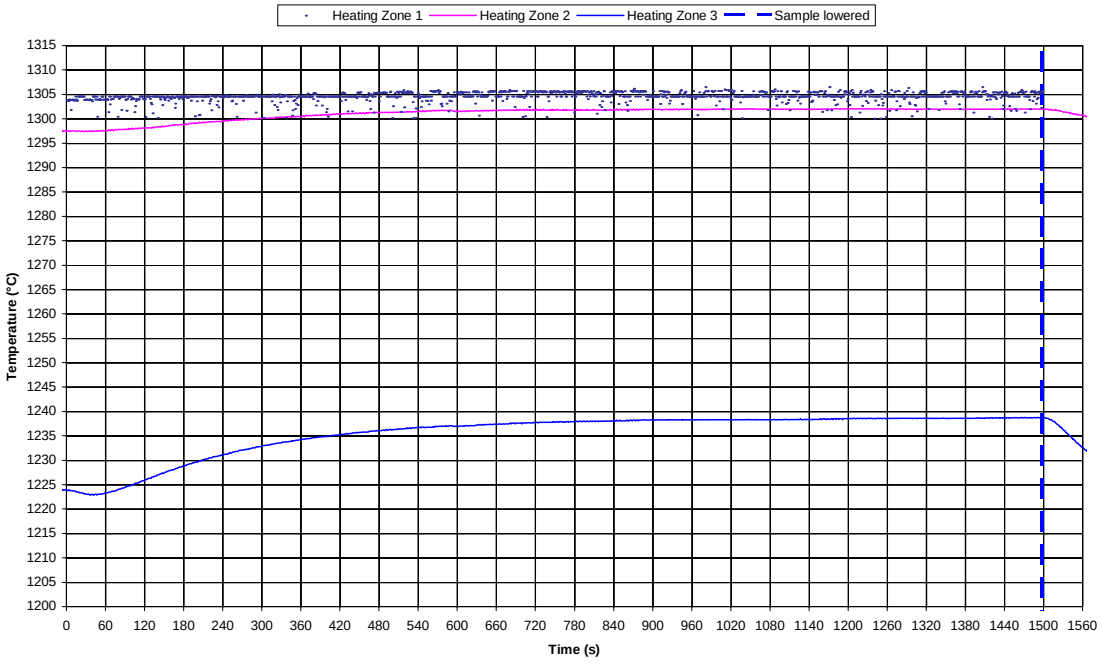

(b) Sample Temperatures (1300A)

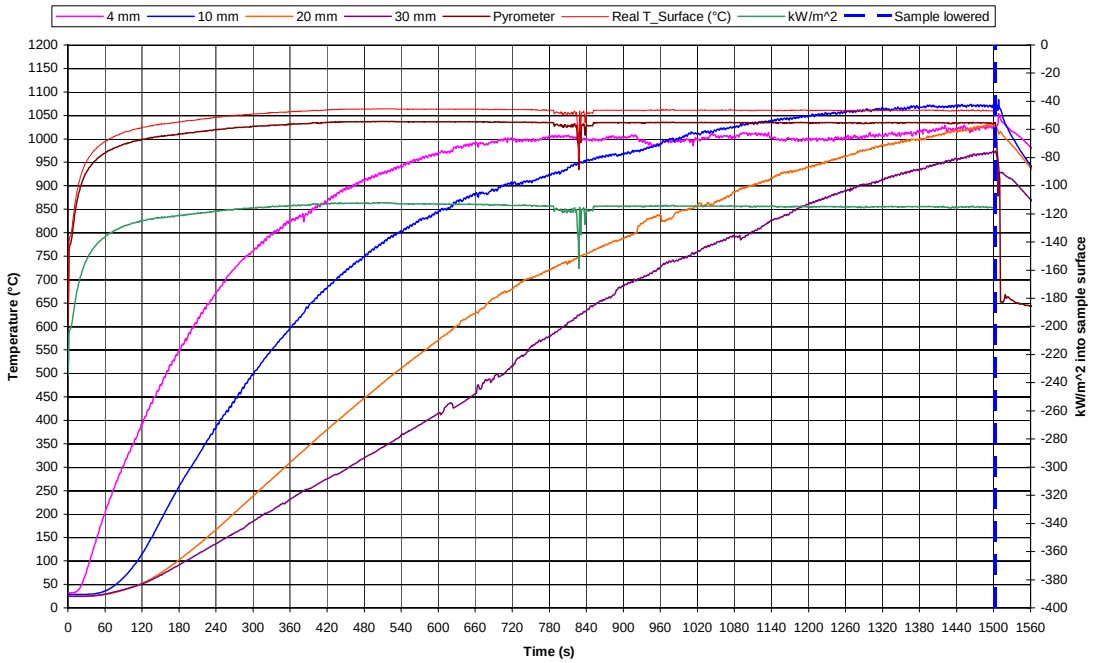

(b) Sample Temperatures (1300B)

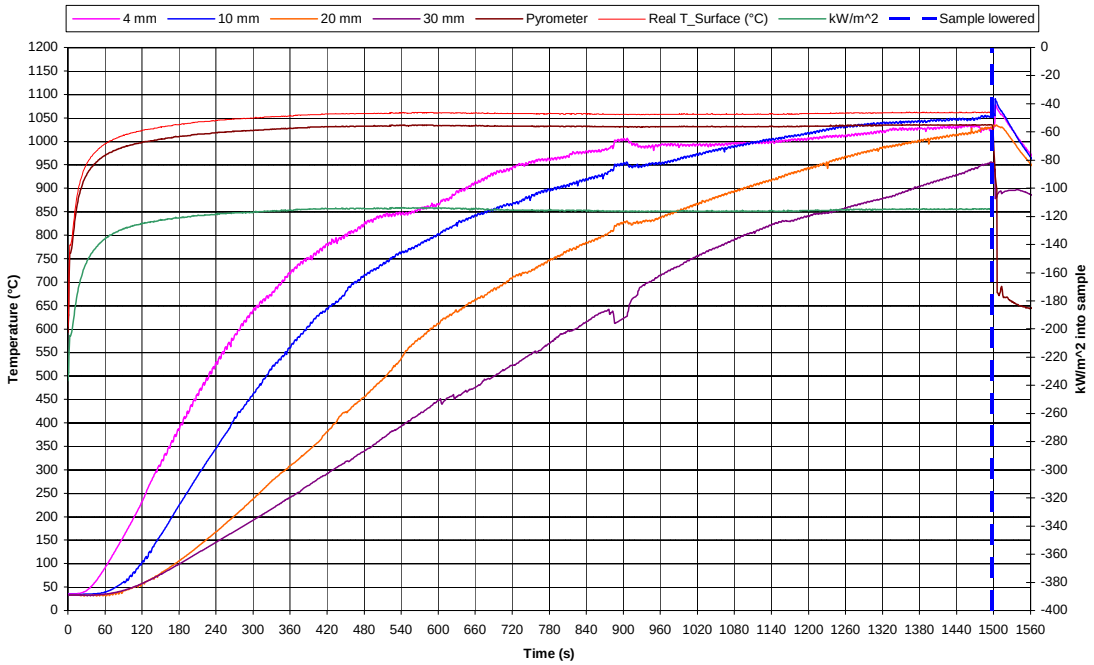

(c) Product Gas Analyses (1300A)

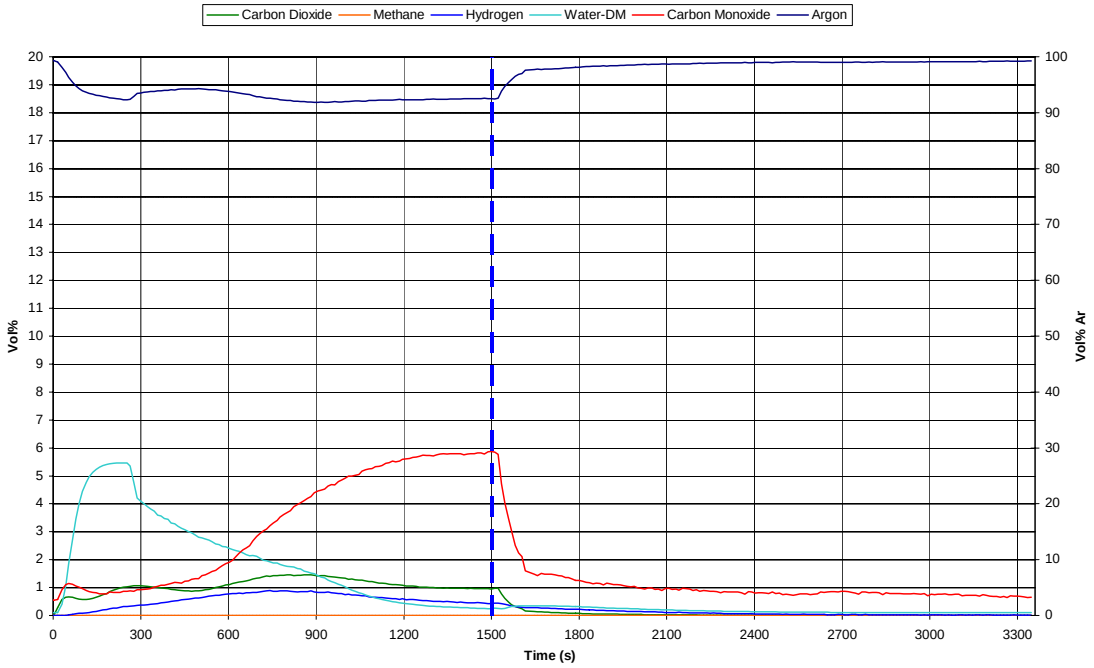

(c) Product Gas Analyses (1300B)

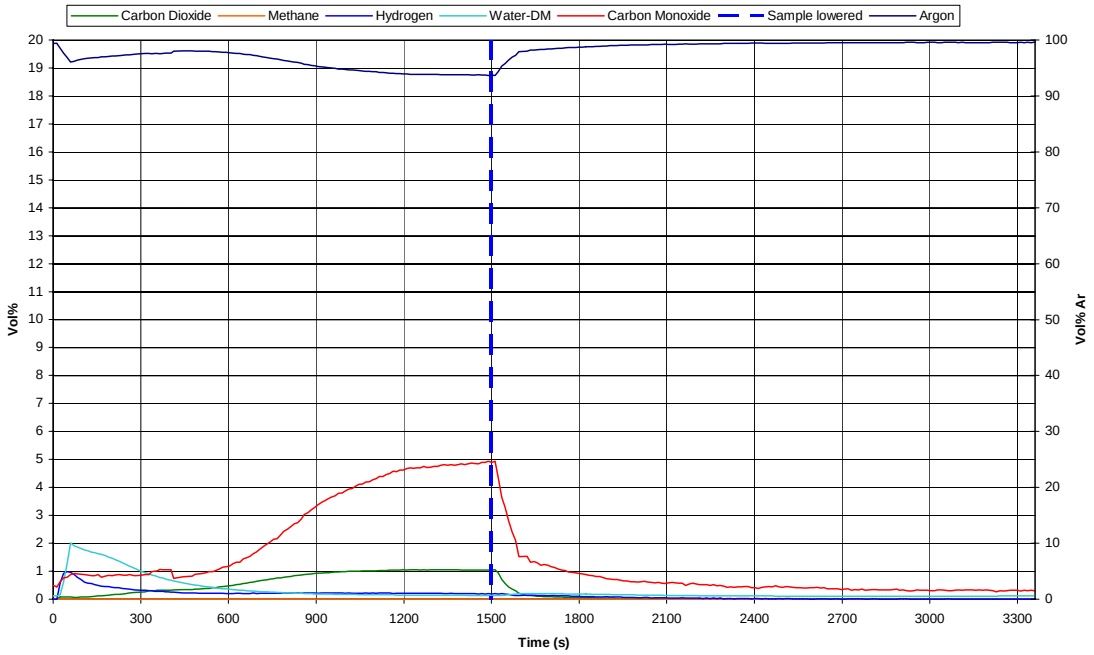

Fig. 18: Calibration Measurements at 1400°C Hot Zone Temperature

(a) Heating Zone Temperatures (1400C)

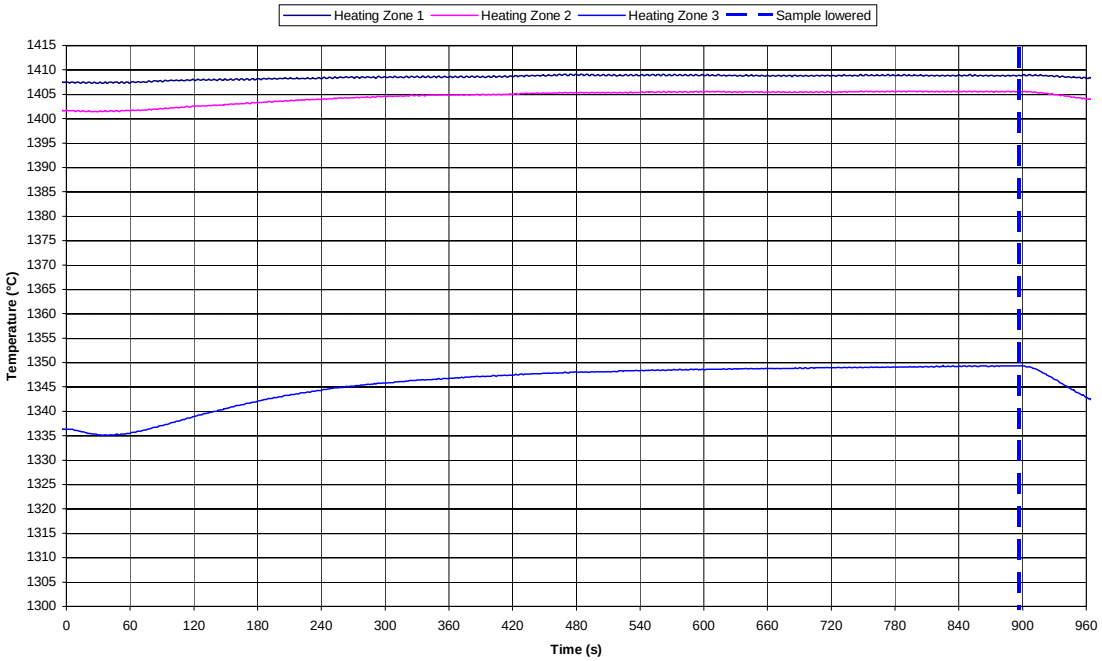

(a) Heating Zone Temperatures (1400D)

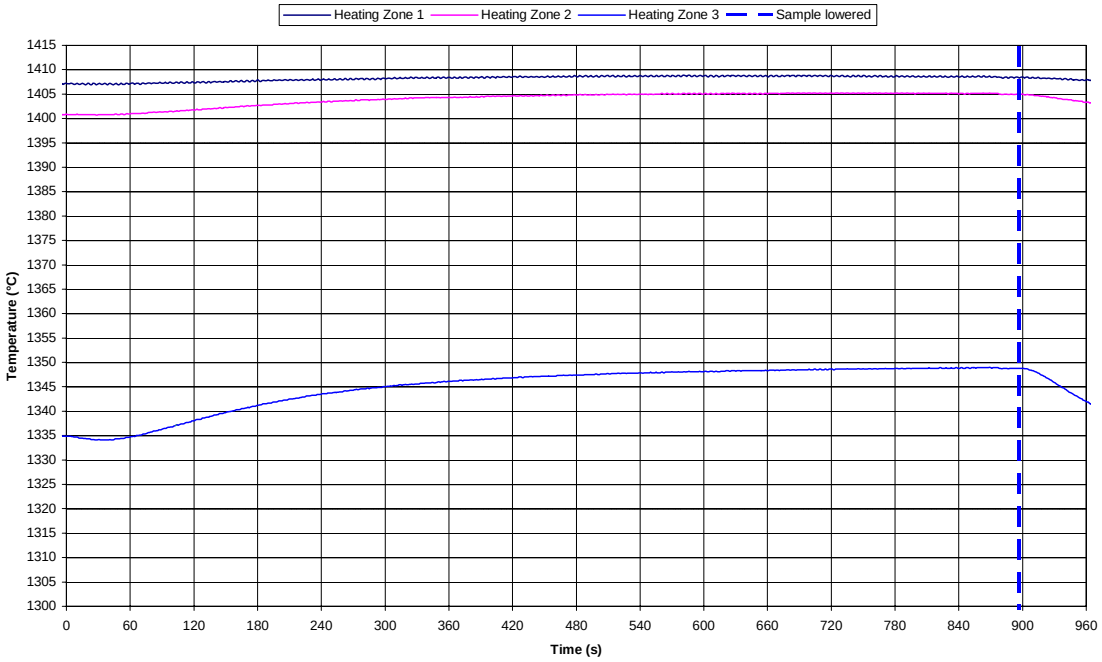

(b) Sample Temperatures (1400C)

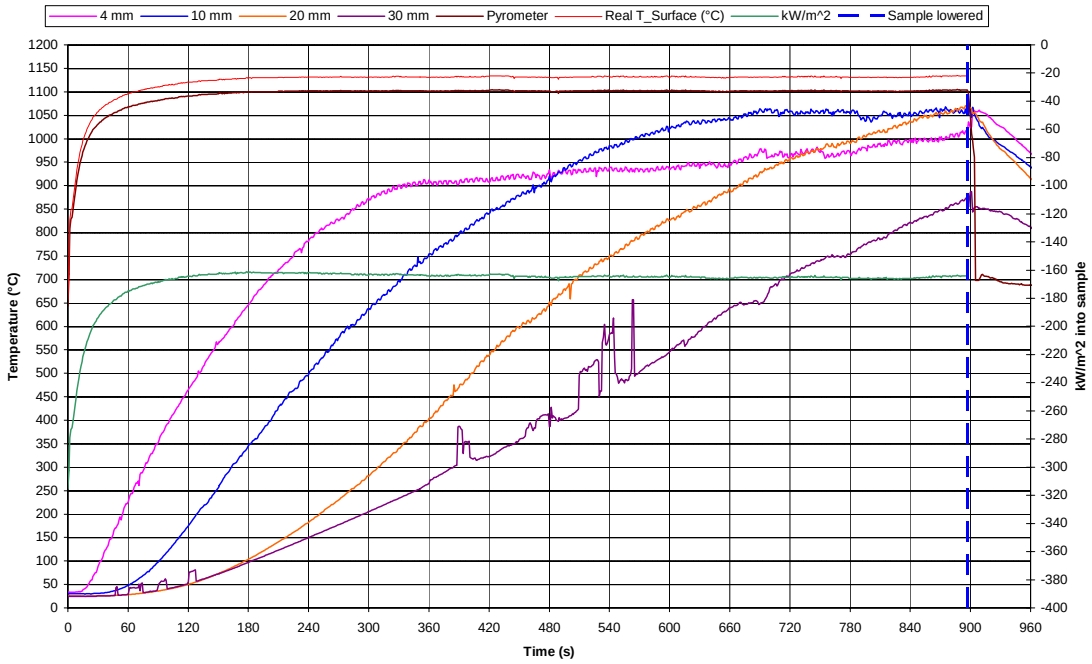

(b) Sample Temperatures (1400D)

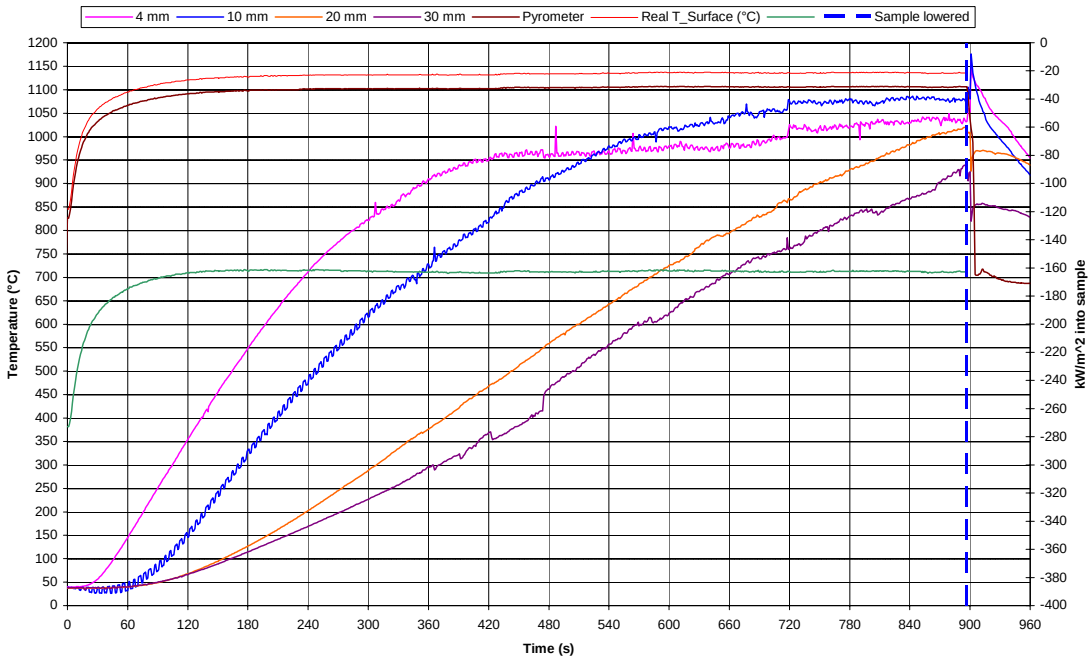

(c) Product Gas Analyses (1400C)

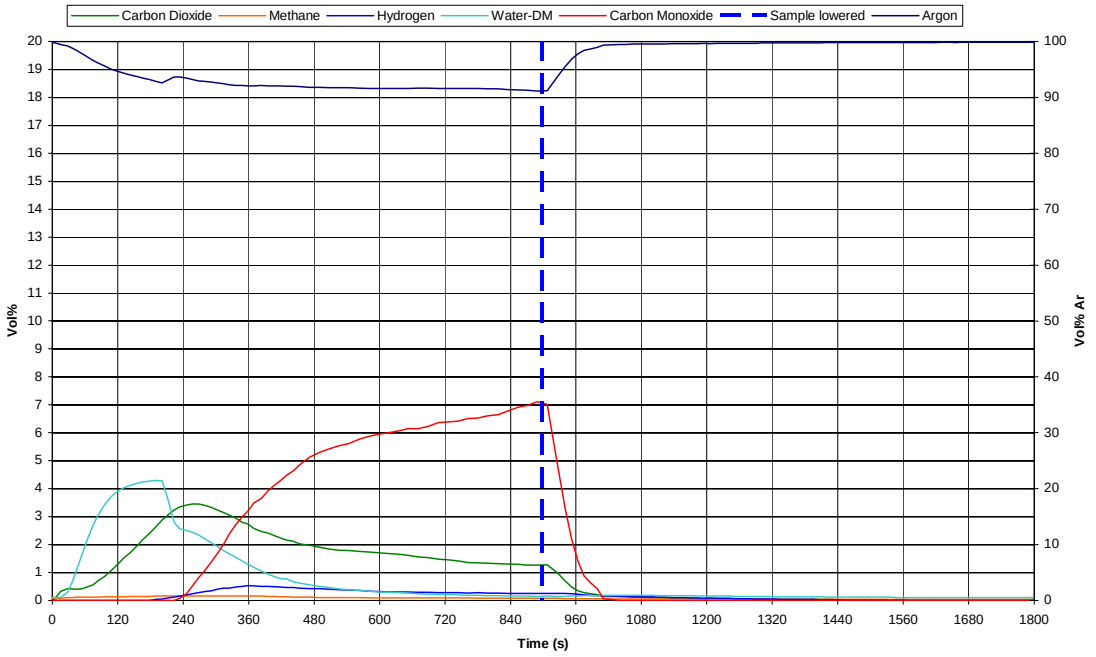

(c) Product Gas Analyses (1400D)

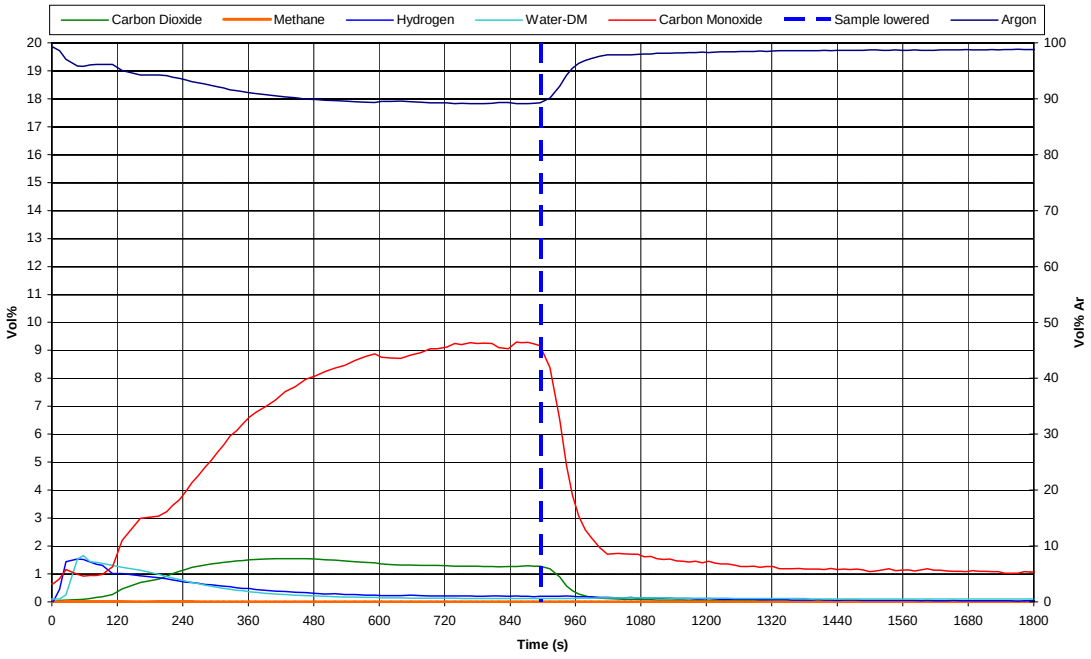

Fig. 19: Calibration Measurements at 1500°C Hot Zone Temperature

(a) Heating Zone Temperatures (1500E)

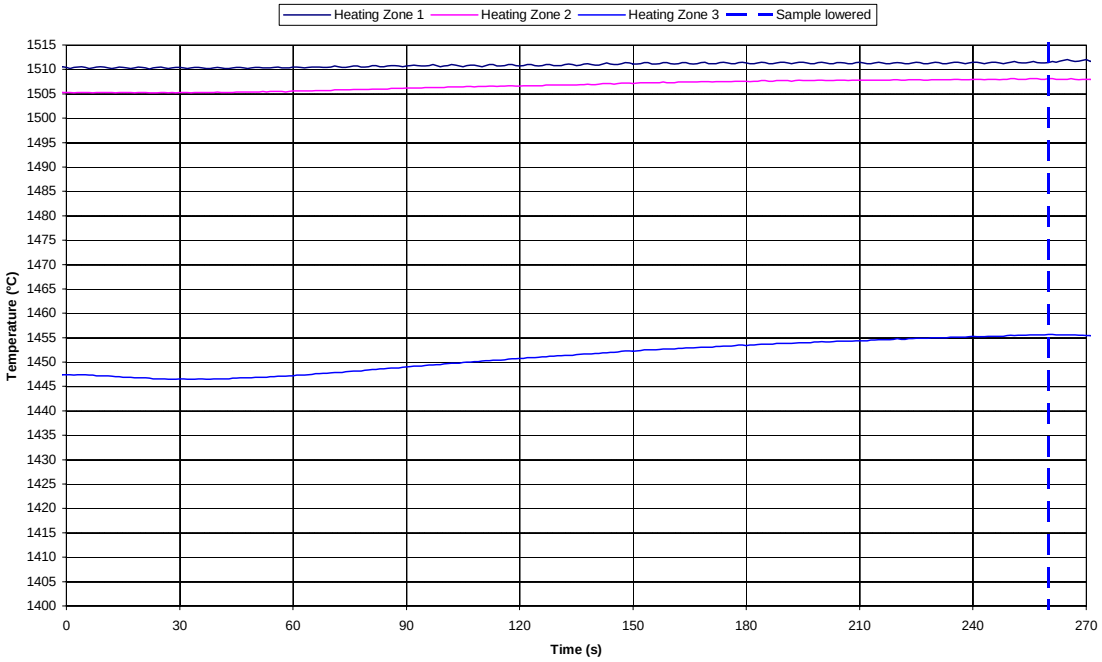

(a) Heating Zone Temperatures (1500F)

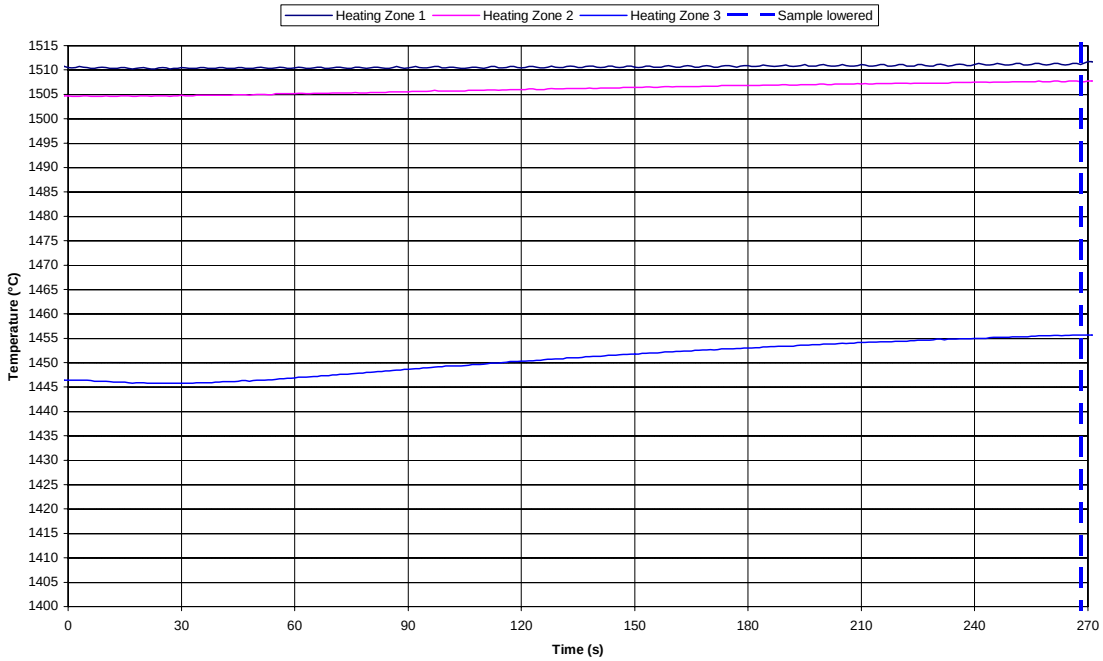

(b) Sample Temperatures (1500E)

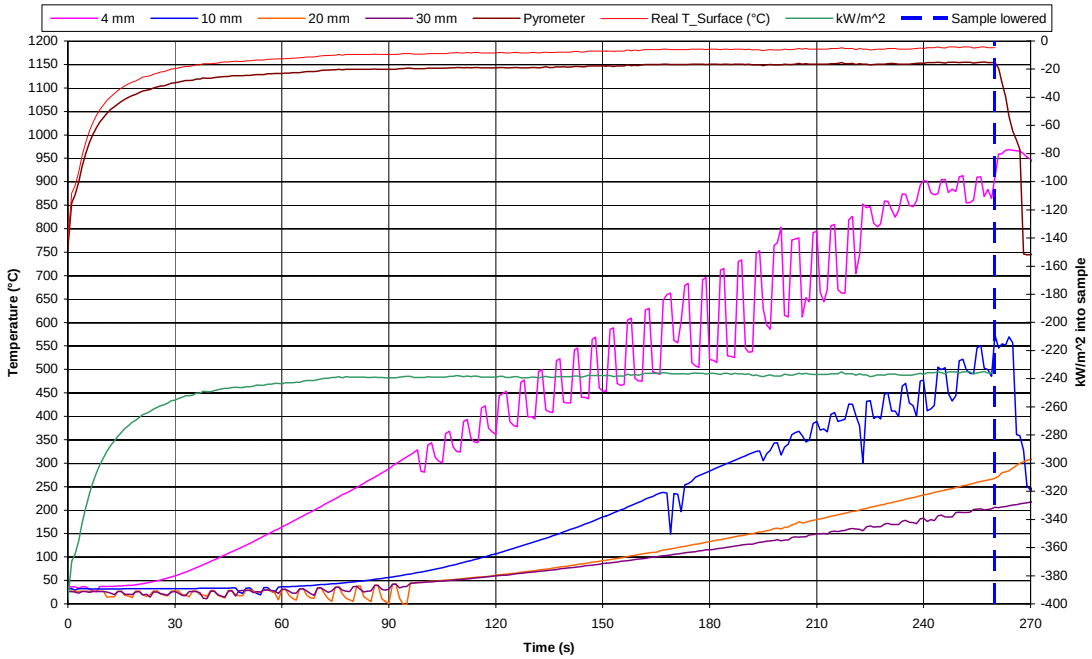

(b) Sample Temperatures (1500F)

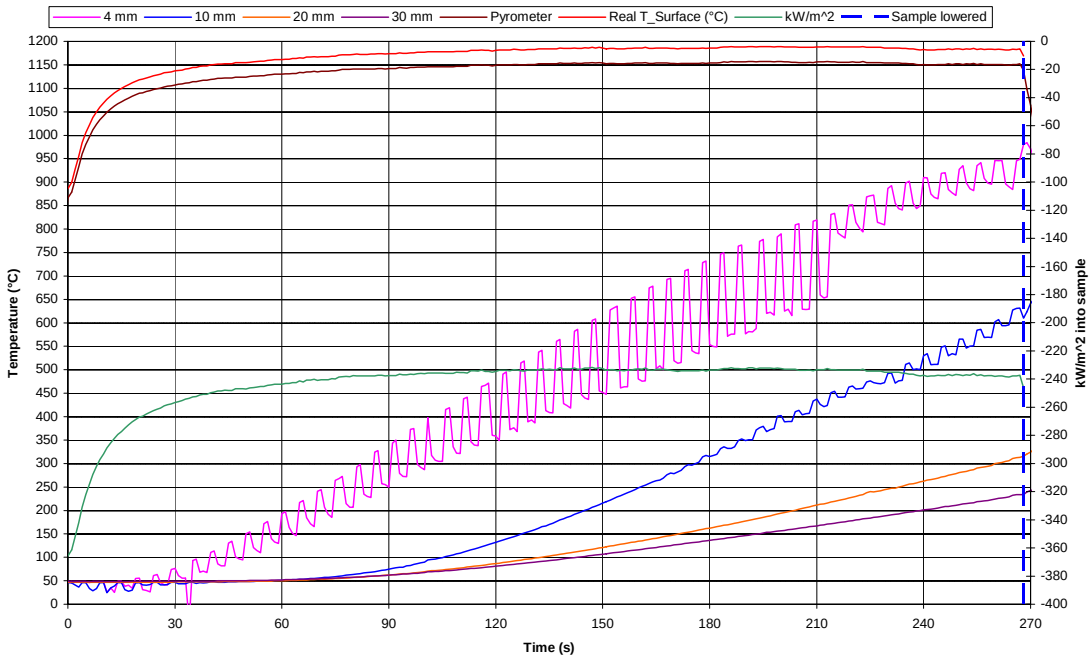

(c) Product Gas Analyses (1500E)

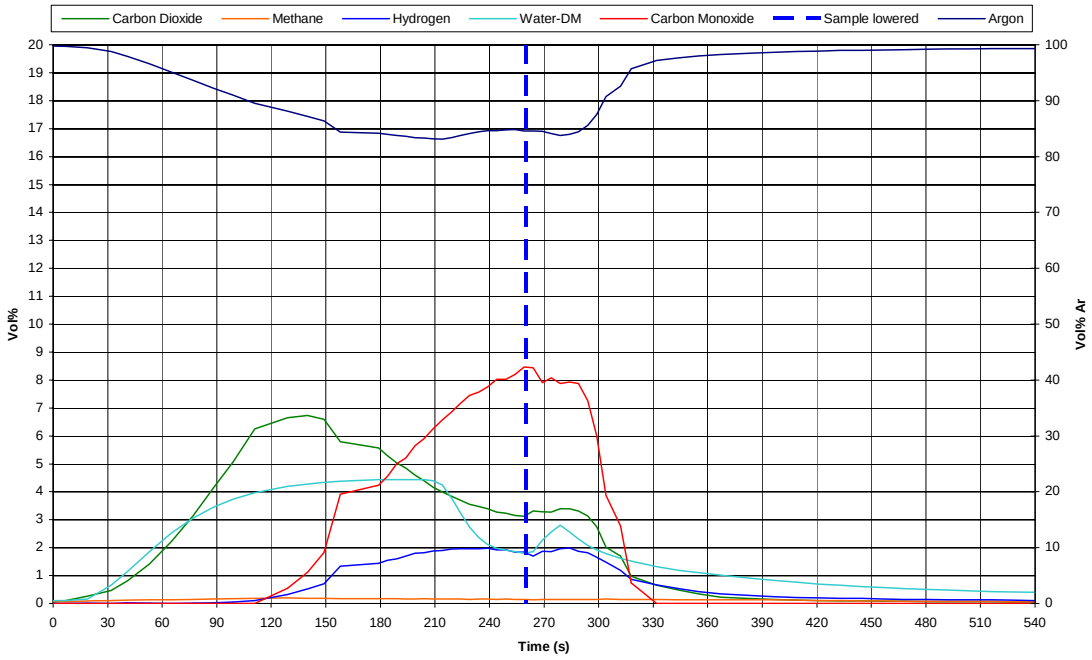

(c) Product Gas Analyses (1500F)

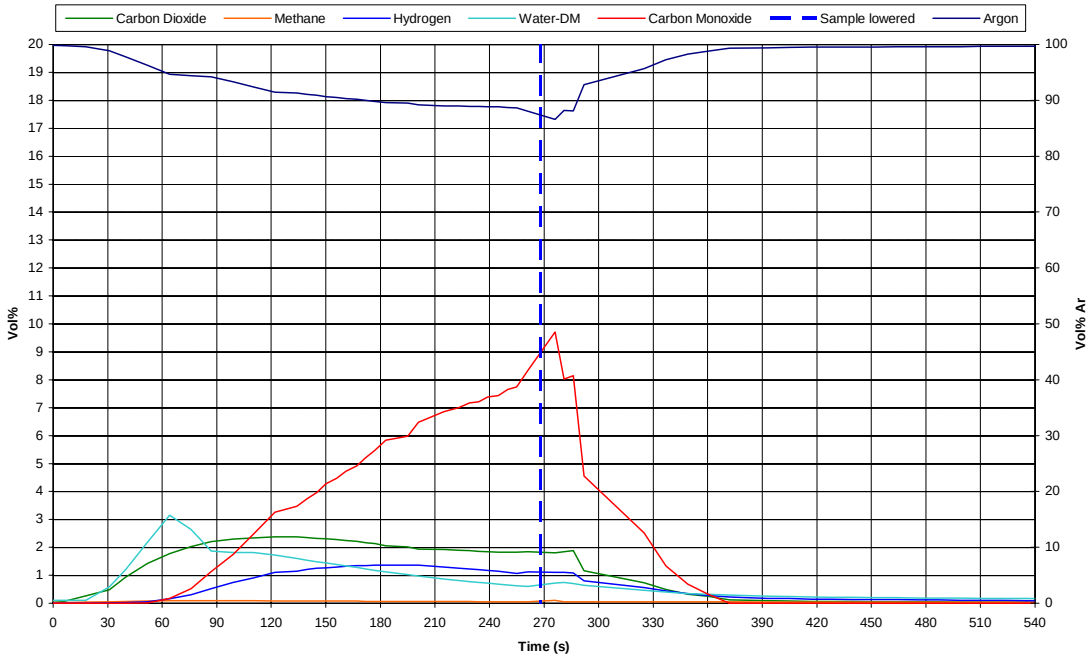

To indicate the sensitivity of the radiation network calculation (of heat transfer to the sample surface), to changes in conditions, the individual measurement parameters were changed and the effect noted. This is shown in **Table 8**. The measurements for the calibration sample 1400C, reacted at 1400°C furnace temperature, were used as basis for the sensitivity calculations. It is seem from **Table 8** that the sample surface emissivity used in the calculation has the biggest influence on the radiation network calculation. For the measured parameters the sample surface temperature and the heating zone 3 temperatures have the biggest effect on the calculated heat transferred to the sample surface. If the correct emissivity value of 0.90 is used for the sample surface, the remaining effect of possible errors in the temperature measurements provides an estimated maximum error of ±19 kW/m^2 for the heat transfer calculation.

Table 8: Radiation network calculation sensitivities

Parameter	Parameter Value Change	Parameter Basis Value	kW/m^2	*ΔkW/m^2
Basis	----	----	-167	0
Measured sample surface temperature (surface 4)	+15°C	1093°C	-159	-8
Measured sample surface temperature (surface 4)	-15°C	1093°C	-176	9
Heating zone No. 1 temperature (surface 1)	+15°C	1409°C	-168	+1
Heating zone No. 1 temperature (surface 1)	-15°C	1409°C	-167	0
Heating zone No. 2 temperature (surface 5)	+15°C	1405°C	-170	+3
Heating zone No. 2 temperature (surface 5)	-15°C	1405°C	-165	-2
Heating zone No. 3 temperature (surface 6)	+15°C	1346°C	-177	+10
Heating zone No. 3 temperature (surface 6)	-15°C	1346°C	-158	-9
Furnace tube emissivity: $\varepsilon_1, \varepsilon_5, \varepsilon_6$	+0.10	0.68	-167	0
Furnace tube emissivity: $\varepsilon_1, \varepsilon_5, \varepsilon_6$	-0.10	0.68	-168	+1
Sample surface emissivity ε_4	+0.09	0.90	-191	+24
Sample surface emissivity ε_4	-0.10	0.90	-141	-26
Bottom radiation shield emissivity ε_3	+0.10	0.53	-167	0
Bottom radiation shield emissivity ε_3	-0.10	0.53	-167	0
Top radiation shield emissivity ε_2	+0.10	0.54	-167	0
Top radiation shield emissivity ε_2	-0.10	0.54	-167	0

*ΔkW/m^2 = (Basis kW/m^2) - (New kW/m^2)

When the sample was cut into the three node sections some fibre board material carry over occurred. The sample masses were corrected for this fibre board carry over by mass balance of the SiO_2 and Al_2O_3 in the sample, using the analyses of %SiO_2 and %Al_2O_3 in the reacted samples, and consequently the sample analyses were corrected for the fibreboard carry over as well. The details of

this calculation are shown in **Appendix VII.** The masses and analyses before and after the correction are shown in **Appendix VI**. The end-point chemical analyses for the calibration samples, the corrected sample node masses out and the end-point temperatures are summarised in **Table 9**.

Table 9: End-point data for calibration samples

Furnace Temperature (°C)	Sample Number	Sample Position	Node End Temperature (°C)	*Node mass out (g.)	*Fibre board mass out (g.)	*%C	%Reduction
1300	1300A	Top	1071	15.4	14.5	12.9	45.4
		Middle	1030	15.4	4.2	13.2	25.5
		Bottom	974	10.7	12.9	15.1	23.9
1300	1300B	Top	1051	18.2	11.2	12.4	38.8
		Middle	1027	14.6	6.9	12.7	25.2
		Bottom	954	8.6	12.9	18.7	24.5
1400	1400C	Top	1054	16.0	11.7	10.5	46.6
		Middle	1071	15.1	7.3	13.5	25.6
		Bottom	874	9.5	13.4	18.0	24.7
1400	1400D	Top	1077	15.1	12.1	12.2	54.8
		Middle	1014	14.8	7.0	11.1	26.1
		Bottom	922	9.7	13.2	16.2	25.2
1500	1500E	Top	909	18.7	11.8	16.8	31.4
		Middle	268	15.4	6.9	12.2	21.2
		Bottom	206	9.1	13.6	13.9	23.3
1500	1500F	Top	981	11.5	5.8	14.6	36.5
		Middle	316	14.5	7.7	14.3	23.0
		Bottom	234	16.9	17.3	13.6	22.9

*Corrected for fibreboard carry-over

The assumptions made in the incremental mass-energy balance calculations are discussed below with reference to **Fig. 20** in which the reaction products are shown. For each time interval the reaction extent and temperature of the solid material and gas products in each node are required.

Fig. 20: Crucible and sample material

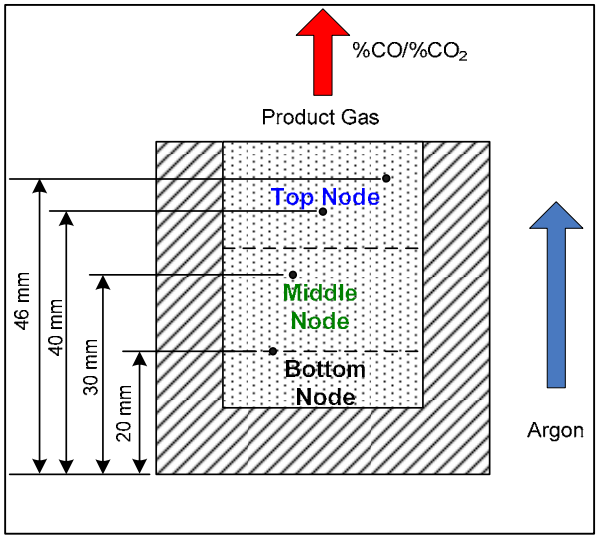

- The sample mass out (on completion of reaction) and the mass Fe out were used in the mass balance calculations. This is acceptable because the mass Fe in to mass Fe out ratio is close to one, as expected and is shown in **Appendix VI**.

- The reduction extent over reaction time is stepwise linear. This linear trend is used to interpolate the reduction extent between the initial input material reduction extent and the reduction extent as analysed in the sample material after total reaction. The reduction extent at the end of each time interval was calculated by re-proportioning of the forms of iron analysis of the input pre-reduced ore material.

- The oxygen removed from the sample must be present in the product gas as CO or CO_2. This assumption is made based on no volatile content in the graphite used as reductant, and little H_2 and H_2O present in the product gas. The carbon balance must be closed by using a CO-CO_2 gas composition from each node to attain the %C calculated equal to that analysed in the reacted node sample. Forms of Fe analyses of the reacted samples show the reduction extent in each node, and from this information it is seen that the middle and bottom nodes do not show further reduction progress from the initial reduction extent. Therefore, the CO and CO_2 in the product gas are generated from the top node only, and are taken to exit the sample at the top node temperature. The mass of oxygen released to the product gas is calculated from the reduction extent in the top node. The product gas %CO/(%CO+%CO_2) ratio is then specified in the heat-mass balance as equal to that at the end of each time interval in the total product gas analysis. The %C remaining in the sample is then a result of the heat-mass balance calculation, and can be compared with that analysed in the reacted sample.

- The total water measured in the product gas analysis is taken as part of the sample and released with the rest of the product gas from the sample at the top node temperature. This assumption is based on the chemical analyses done on the reacted material, which shows that most of the reduction takes place in the top node. Water release from the sample over time was proportioned according to the water content analysed in the product gas.

- The temperatures measured by the four thermocouples positioned in the material layer are assigned to the three node segments as follows: the top node is at the end-point temperature measured by the thermocouple positioned 10 mm from the sample surface; the middle node is at the end-point temperature of the thermocouple which is 20 mm from the sample surface; and the bottom node is at the end-point temperature of the thermocouple which is 30 mm from the sample surface. It is seen from the sample temperature graphs in **Fig. 17-19 (b)** that the thermocouple positioned 4 mm from the sample surface, for longer experiment times at 1300°C

and 1400°C, levels off and the thermocouple values are lower than that for the thermocouple at 10 mm and/or 20 mm from the sample surface. The material bed level lowers throughout the experiment, so that the top thermocouple may not be covered by material at the end of the experiment, and thus temperature values from the top thermocouple are not reliable towards the end of the experiment. For the tests done at 1500°C a short reaction time was used because of slag formation. For these two tests, the thermocouple positioned 10 mm from the sample surface is much lower than the thermocouple positioned 4 mm from the sample surface. Therefore, the latter temperature is used for the top node for these two samples reacted at 1500°C furnace temperature.

- In the mass and energy balance several factors must be taken into account, besides the end-point material temperatures discussed above. The heat transferred to the sample also heats up the thermocouples embedded in the sample, as well as the crucible material. The masses for the crucible material can be proportioned between the three nodes, using the mass measurements made when the sample was cut into the three node portions. The thermocouple material must be roughly estimated from mass measurements of alumina sheaths cut to the length of the thermocouples embedded into the sample. The latter masses are small compared to that of the crucible material, and were therefore not considered in the heat-mass balance. The crucible material consists of 65% Al_2O_3 and 35% SiO_2, and was considered to be mullite in the heat-mass balance calculations.

- The other factor to take into account for the heat mass balance is the heat transferred to the Ar carrier gas used. This is factored into the heat-mass balance by assuming that the Ar is heated to the top node temperature. The Ar gas flow rate for each time increment was calculated by proportioning the total Ar flow rate for each time increment.

The incremental heat-mass balance calculation sheets for sample 1400C are shown in **Appendix VI**. The sensitivities of the above assumptions for sample 1400C are summarised in **Table 10**. Comparison of the heat transfer values calculated from the heat-mass balance to that calculated in the radiation network is shown in **Table 11** and **Fig. 21**. Reduction extent for the top segment is shown in **Fig. 22**. Comparison of the %C in the reacted sample with that analysed is shown in **Fig. 23 a-c**. The data values in the figures are shown at the furnace temperatures offset by 5°C to facilitate clarity of the graphs. It is seen that for the experiments at 1300°C and 1400°C furnace temperature the calculated mass-heat balance kW/m^2 values and those calculated from the radiation network correspond well. However, for the experiment 1500F reacted at 1500°C there is a difference of 22% of the value calculated from the incremental heat-mass balance. From **Fig. 23 a-c** it is seen that the calculated and

analysed %C remaining in the sample differ by a maximum of 7% for the top node of sample 1500F. In terms of the total initial mass carbon input of 3.0 g into the sample top node, 7% is 0.2 g.

Table 10: Heat-mass balance sensitivities for sample 1400C

Condition	kW/m^2 calculated from heat-mass balance	kW/m^2 calculated from radiation network
+Ar; +FB, +H_2O	-163	-167
+Ar; +FB, -H_2O	-158	---
+Ar; -FB, +H_2O	-109	---
-Ar; +FB, +H_2O	-131	---
+Ar at 500°C; +FB, +H_2O	-146	---
+Ar; +FB, +H_2O, 100%CO in CO-CO_2 product gas	-167	---
+Ar; +FB, +H_2O, 100%CO_2 in CO-CO_2 product gas	-159	---
+Ar; +FB, +H_2O, sample solids temperatures +50°C	-171	---
+Ar; +FB, +H_2O, sample solids temperatures -50°C	-155	---

+Ar = Argon carrier gas included in heat-mass balance
+FB = Fibreboard crucible material included in heat-mass balance
+H_2O = Water in product gas analysis included in heat-mass balance

Table 11: Heat transfer values comparison

Sample No.	kW/m^2 calculated from incremental heat-mass balance	kW/m^2 calculated from radiation network	*Difference in kW/m^2	Difference as % of kW/m^2 calculated from incremental heat-mass balance
1300A	-110	-118	8	7
1300B	-107	-118	11	10
1400C	-163	-167	4	2
1400D	-166	-166	0	0
1500E	-245	-245	0	0
1500F	-200	-243	43	22

*Difference in kW/m^2 = (kW/m^2 calculated from incremental heat-mass balance) - (kW/m^2 calculated from radiation network)

Fig. 21: Heat transferred to sample

(Experimental period at 1500°C furnace temperature is 4.5 minutes only)

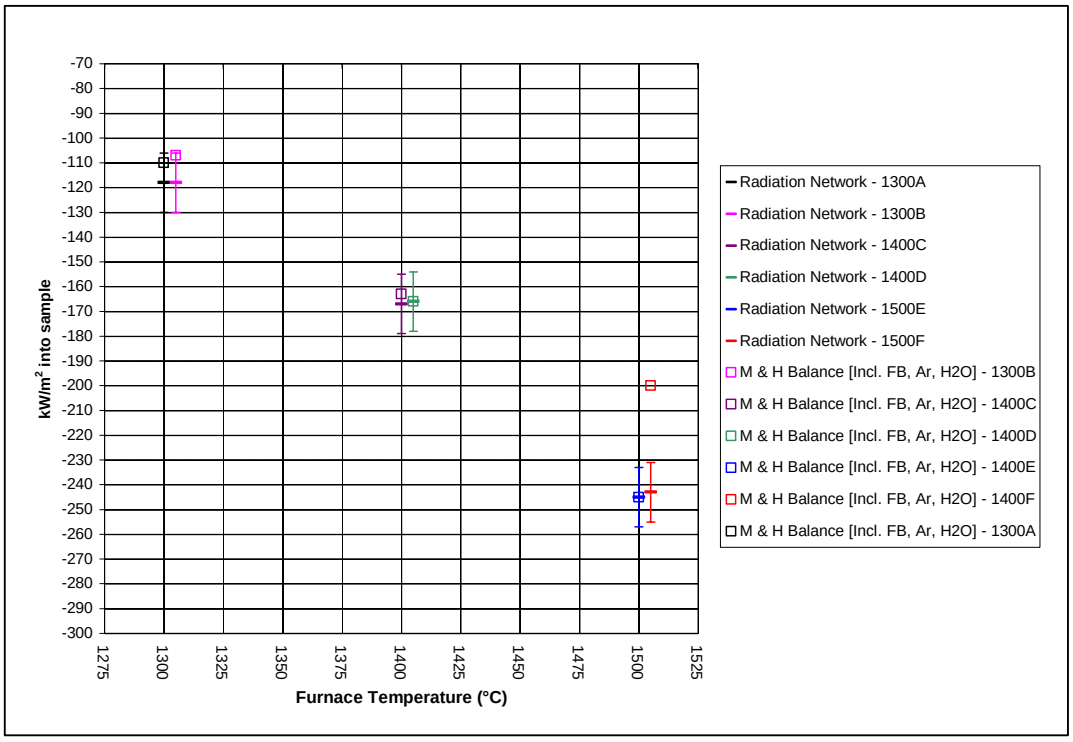

Radiation Network = weighted average kW/m^2 heat transferred to sample as calculated from radiation network

M & H Balance = weighted average kW/m^2 heat transferred to sample as calculated from incremental heat – mass balance

Fig. 22: %Reduction in top segment

(Experimental period at 1500°C furnace temperature is 4.5 minutes only)

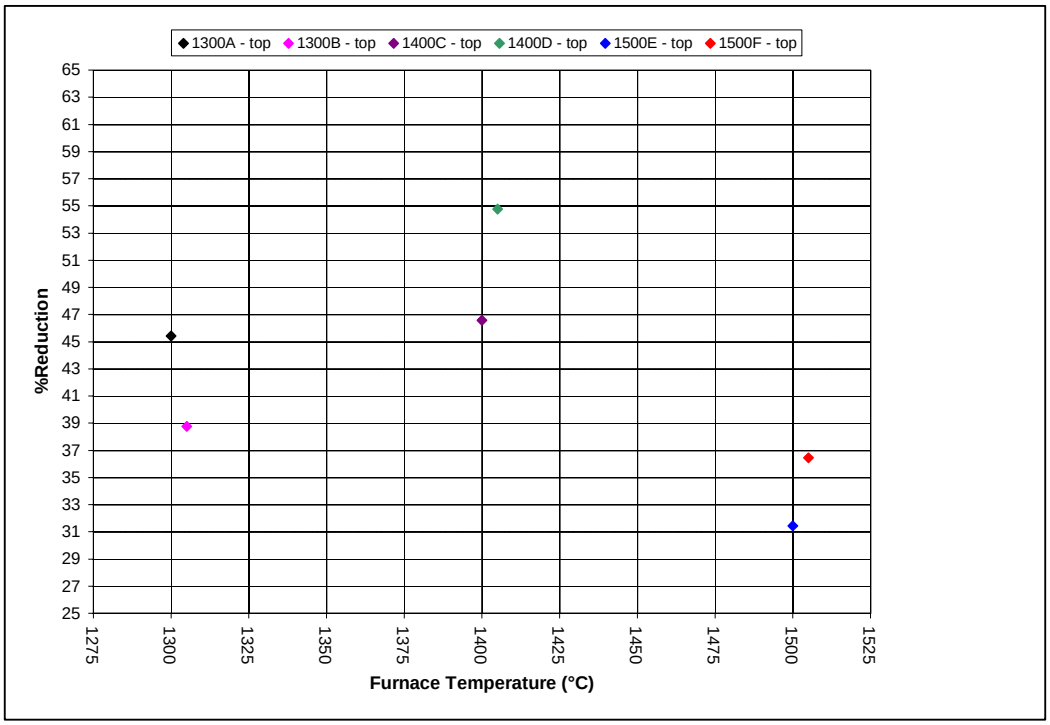

Fig. 23: %C analysed vs. calculated from heat-mass balance

(a) Top node

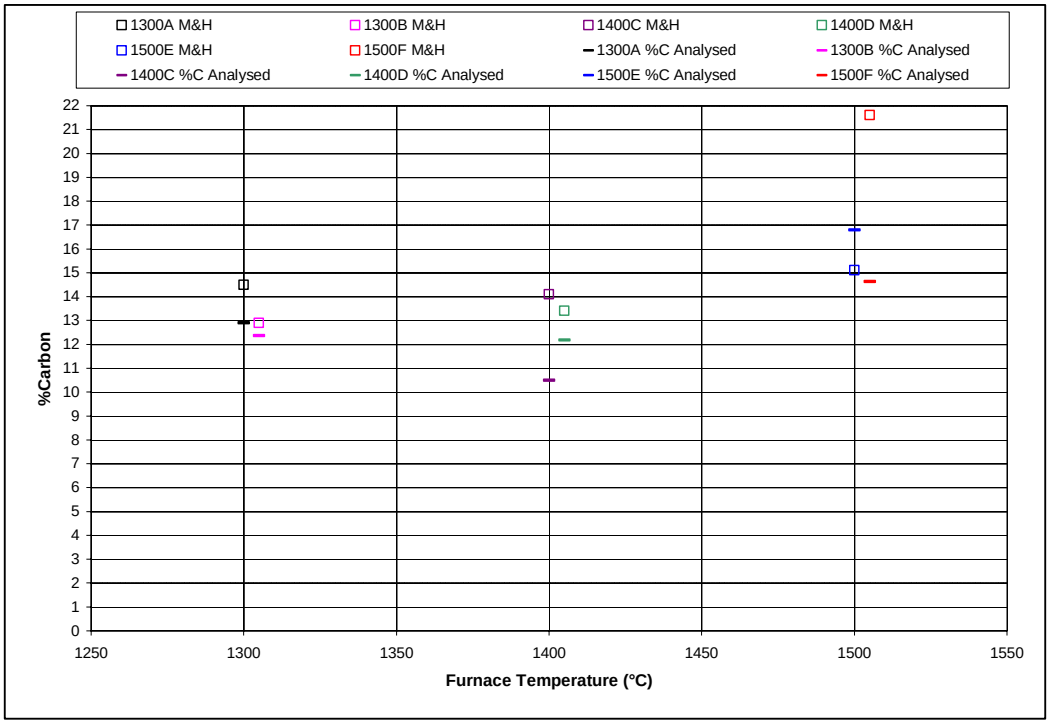

(b) Middle node

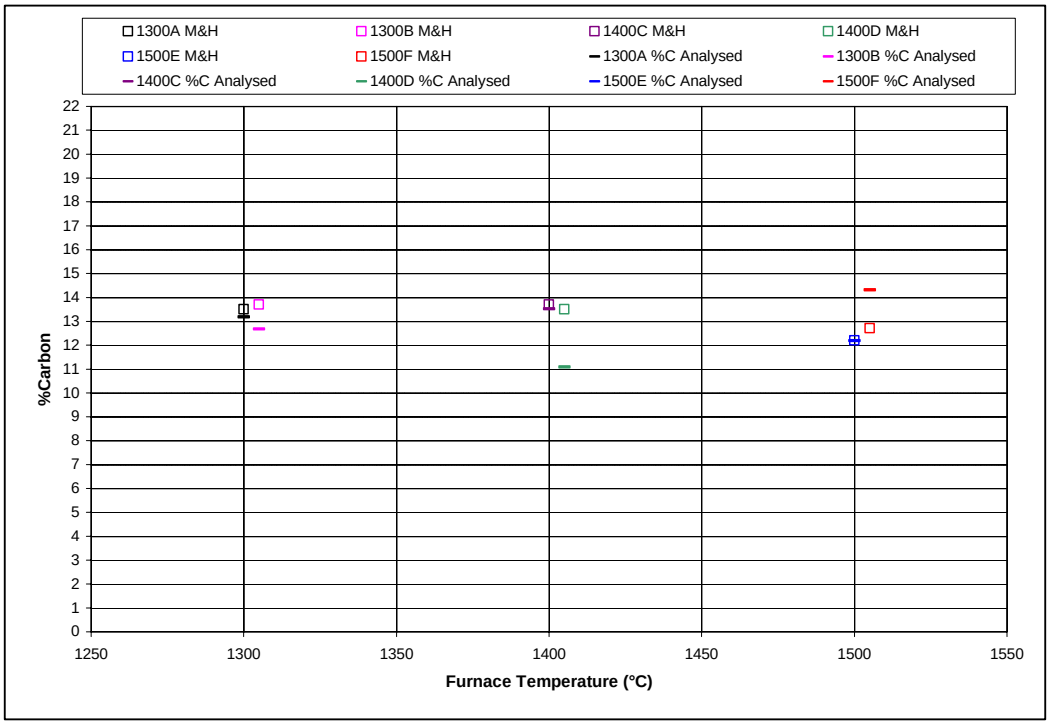

(c) Bottom node

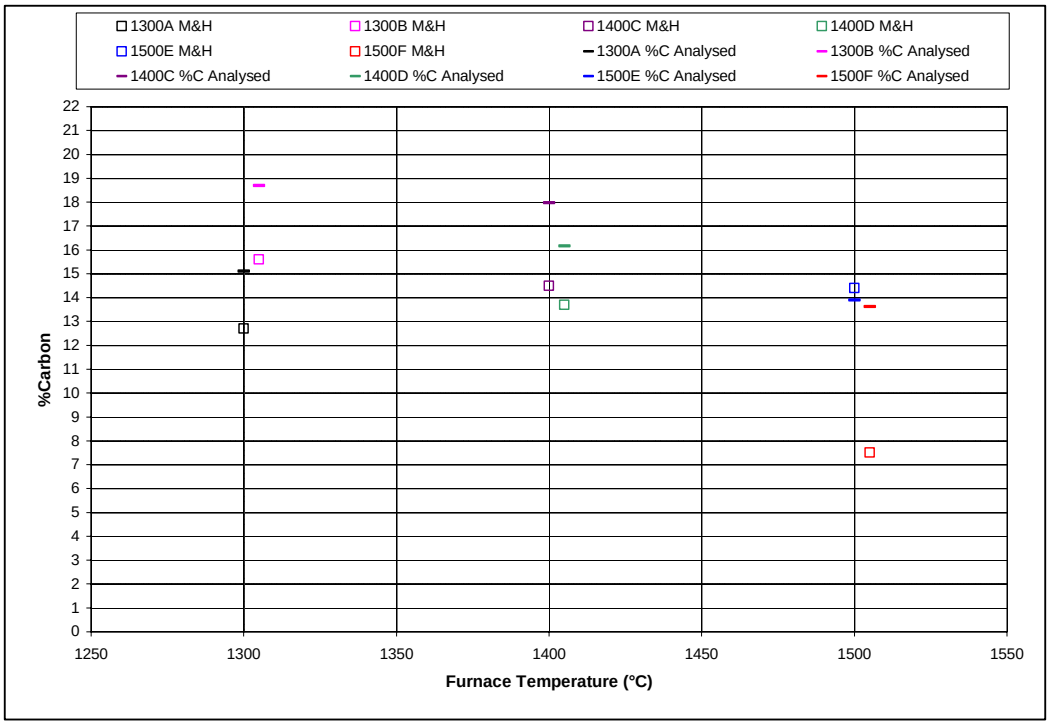

2.3. Conclusion

The experimental set-up is appropriate for quantifying radiation heat transfer to samples reacted non-isothermally in this set-up. The heat-mass balance calculations and the radiation heat transfer to the sample, as calculated from the radiation network, correspond within the radiation network calculation uncertainty for samples reacted at 1300°C and 1400°C furnace temperatures. For samples reacted at 1500°C furnace temperature, the difference is larger due to the short reaction time and resultant small reaction extent achieved in these samples. The sample cutter-splitter allows for the repeatable division of the reacted sample into three node portions for further chemical analysis.